SCIENCE CHINA
Earth Sciences

•REVIEW•

May 2022 Vol.65 No.5: 783–809
https://doi.org/10.1007/s11430-021-9893-8

Tsunami hazard assessment in the South China Sea: A review of recent progress and research gaps

Linlin LI[1,2], Qiang QIU[3,4,5*], Zhigang LI[1,2] & Peizhen ZHANG[1,2]

[1] *Guangdong Provincial Key Laboratory of Geodynamics and Geohazards, School of Earth Sciences and Engineering, Sun Yat-sen University, Guangzhou 510275, China;*
[2] *Southern Marine Science and Engineering Guangdong Laboratory (Zhuhai), Zhuhai 519082, China;*
[3] *CAS Key Laboratory of Ocean and Marginal Sea Geology, South China Sea Institute of Oceanology, Innovation Academy of South China Sea Ecology and Environmental Engineering, Chinese Academy of Sciences, Guangzhou 510301, China;*
[4] *Southern Marine Science and Engineering Guangdong Laboratory (Guangzhou), Guangzhou 511458, China;*
[5] *China-Pakistan Joint Research Center on Earth Sciences, CAS-HEC, Islamabad 45320, Pakistan*

Received August 20, 2021; revised December 29, 2021; accepted January 25, 2022; published online March 25, 2022

Abstract The South China Sea region is potentially threatened by tsunami hazards originated from multiple sources: the Manila subduction zone in the east, the Littoral Fault Zone (LFZ) in the north, numerous submarine landslides on the continental slopes and the volcanic islands in the Luzon Strait. Infrequent but potentially devastating tsunami hazard poses a great threat to the populous coastal region, fishery, oil and gas exploitation in the deep sea, etc. Here we review the recent progress in tsunami hazard assessment in the South China Sea region, focusing on two primary sources: submarine earthquakes and landslides. We sort and review the literature by the two commonly used approaches: deterministic and probabilistic tsunami hazard assessment for both source types. By simulating tsunamis generated by typical earthquakes originated from the Manila Trench, the LFZ and landslides in the continental slopes, we investigate their tsunamigenic mechanism and key tsunami characteristics in the South China Sea region. We point out the research gaps and highlight the key issues to be addressed in the future.

Keywords Tsunami, Submarine earthquake, Submarine landslide, the Littoral Fault Zone

Citation: Li L, Qiu Q, Li Z, Zhang P. 2022. Tsunami hazard assessment in the South China Sea: A review of recent progress and research gaps. Science China Earth Sciences, 65(5): 783–809, https://doi.org/10.1007/s11430-021-9893-8

1. Introduction

Tsunamis are infrequent but potentially devastating events, among one of the deadliest marine geohazards. Tsunamis are usually triggered by submarine earthquakes, submarine landslides, volcanic activities and meteorites, etc. The M_W9.1 2004 Sumatra-Andaman earthquake and tsunami is a milestone event in tsunami research. This earthquake triggered a transoceanic tsunami which devastated the coastal countries surrounding the Indian Ocean, causing nearly 230,000 death and 12 billion USD economic losses (Titov et al., 2005). Only seven years later, the 2011 Tohoku-Oki earthquake (M_W9.0) triggered another transoceanic tsunami in the Pacific Ocean, causing 27,000 death or missing in Japan and 305 billion USD economic loss worldwide. The catastrophic effect of this disaster is significantly exacerbated by the damage to the Fukushima nuclear power plant, raising global concerns about the potential effects of the released radiation (Nanto et al., 2011). The rupture zones and magnitudes of these two massive earthquakes challenge the traditional perspective of earth scientists on the seismogenic mechanism of megathrust faults at global subduction zones. Besides the large earthquakes occurring at the subduction interfaces, recent tsunami events raised the awareness that tsunamis

* Corresponding author (email: qiu.qiang@scsio.ac.cn)

could be generated by diverse sources with some of them unexpected. For example, the September 28th, 2018 Sulawesi tsunami was associated with a M_W7.5 strike-slip earthquake, killing more than 1300 people in Indonesia (Schambach et al., 2021). The December 22nd 2018, Anak Krakatau tsunami event was triggered by the flank collapse (0.1–0.2 km^3) of the Anak Krakatau volcano, causing 437 deaths in Indonesia (Williams et al., 2019; Ye et al., 2020). The M_W6.9 Samos normal-faulting earthquake generated nearly 4 m tsunami waves in the populous area in the Aegean sea in Europe (Dogan et al., 2021). Such "atypical" tsunami sources remind us that the complexity and diversity of tsunamigenic mechanisms. The tsunami hazard level could not be simply assessed from the fault mechanism or magnitude of the source earthquakes and the volumes of landslides. Earthquakes with the moderate magnitude or landslides with limited volumes could also generate devastating tsunami event if they occur in unfavoured situations. This fact leads the majority of coastlines globally not immune to potential tsunami hazards.

The coastlines of the South China Sea (SCS) are particularly vulnerable to tsunami hazards due to the following reasons: (1) Many populous cities are distributed along the coastlines. Some cities are among the most economically active centers in their own countries. E.g., with only 0.6% of the national-territorial area, the Guangdong-Hong Kong-Macao Greater Bay Area contributes 12.57% GDP in China; (2) The coastlines also have many major infrastructures including harbors, airports and nuclear power plants, etc. Taking the nuclear power plant as an example, nearly 10 nuclear power plants either under construction or operation are located in the coastal areas of Guangdong, Guangxi, Fujian and Hainan provinces, accounting for half of the total number of power plants in the coastal region in China; (3) The coverages of the infrastructures inside the deep sea including oil platforms and submarine cables are expanding rapidly; (4) The average elevations of coral islands inside the SCS are only several meters above the mean sea level. With many identified landslides nearby, the tsunami waves can arrive at these islands and coastal regions in minutes or tens of minutes once being generated. Consequently, improving our capabilities of emergency response and disaster resistance is imperative. For the recent progress on tsunami early warnings, please refer to An (2021) and Yu et al. (2020).

The formation and evolution of the SCS are governed by the tectonic activity of the surrounding subduction system in the west, south, and east. Under the influence of the subducting Manila trench, active submarine faults and high sediment accumulation rate, diverse marine geo-hazards with different severity levels are present from the continental shelf to the continental slope and deep basin. Earthquakes, landslides and turbidity flows are among the most dangerous types. As the SCS is a semi-enclosed basin, previous studies have shown that tsunamis generated outside the basin can hardly affect the coastlines bordering the SCS (Okal et al., 2011; Yu et al., 2020; An, 2021). As a result, we shall focus our attention to the potential tsunami sources inside the SCS (Figure 1), which include the Manila subduction zone (Megawati et al., 2009; Hsu et al., 2016; Qiu et al., 2019), the Littoral Fault Zone (LFZ) (Ren et al., 2016; Cao et al., 2018; Xia et al., 2020), other active faults in the northern SCS and submarine landslides widely distributed on the continental slope and carbonate platforms (Gee et al., 2007; Li W et al., 2014a; Chen et al., 2016; Sun et al., 2018a; Wang et al., 2018; Wu et al., 2018) and a series of volcanic islands (Terry et al., 2017).

For the above-mentioned tsunami sources, lots of studies have been done in recent years. Here we summarize the important progress in the tsunami hazard assessment of the submarine earthquakes and landslides in the SCS. Meanwhile, we discuss the seismogenic mechanism of the Manila megathrust fault and the LFZ based on their geological structures and available geophysical data. The key features of tsunami impact associated with these sources are demonstrated through simulation results of typical scenarios. Finally, we identify the research gaps and offer suggestions for future research directions. We expect this contribution could provide the scientific basis for tsunami hazard preparation and mitigation in the SCS.

2. Tsunami hazard assessment for the Manila Trench

The Manila subduction zone (MSZ) has been the major subject of tsunami hazard studies since it has the highest potential for generating great earthquakes and tsunamis. The trench is characterized by three typical features: (1) The subduction zone is seismically very active but absent of great earthquakes. No earthquakes larger than M_W7.6 have been recorded along the trench since the Spanish colonization of Luzon in 1560. The absence of significant megathrust related earthquakes suggests that the megathrust is either creeping in the form of slow slip events and slow silent earthquakes (Obana and Kodaira, 2009; Wallace et al., 2016) or accumulating strain energy which could be released during next great or giant earthquakes (Yokota et al., 2016). (2) the coupling ratio of the megathrust is likely up to 0.48 or even higher. Hsu et al. (2016) estimated the coupling ratio through the block modeling, which is constrained by the-20-years' (1998–2015) continuous GNSS observations deployed in Taiwan, China and the Philippines. (3) The convergence rate across the Manila subduction zone is 65–100 mm yr^{-1} (Hsu et al., 2012, 2016). The rate is even higher than those of very active subduction zones which have hosted giant earthquakes in the past i.e., 62–81 mm yr^{-1} of the Japan trench,

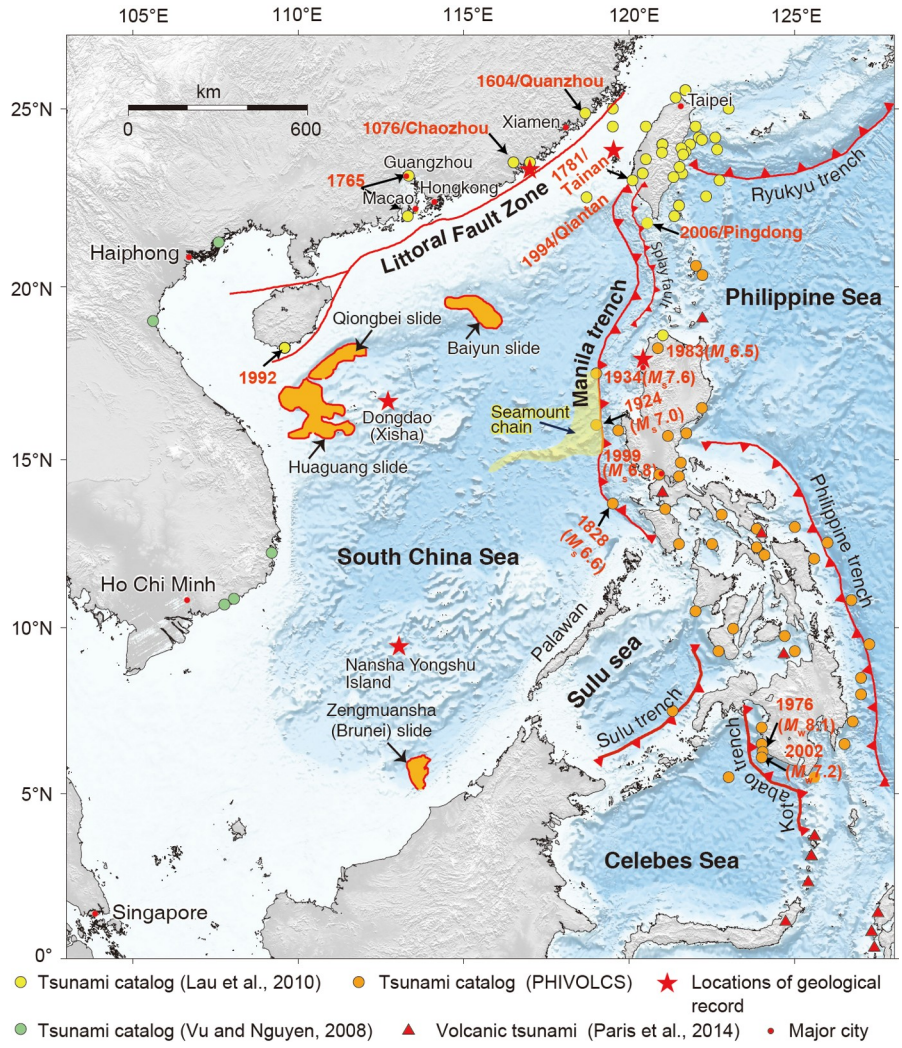

Figure 1 The spatial distributions of the historical and geological tsunami records and potential tsunami sources in the SCS. Yellow dots indicate the tsunami records in the northeast of the SCS (Lau et al., 2010). Red triangles mark the tsunami records with possible volcanic origins in southeast Asia (Raphaël Paris et al., 2014). Green dots represent tsunami records in Vietnam (Vu and Nguyen, 2008). Orange dots mark the tsunami records collected by Philippine Institute of Volcanology and Seismology during 1589–2012 (Bautista et al., 2012). Red pentagrams represent the locations of possible tsunami deposits. The boundaries of the Baiyun slide are digitized from Sun et al. (2018b), Qiongbei slide and Huaguang slide are from Wang et al. (2018), Zengmuansha (Brunei) slide is from Gee et al. (2007). This figure is modified from Qiu et al. (2019).

50–60 mm yr^{-1} (Chamot-Rooke and Le Pichon, 1999) of the Sumatran and 58–72 mm yr^{-1} of the Chilean subduction zones (McCaffrey, 2008). These typical features imply that the potential risk of imminent great or giant earthquakes could not be ruled out along the Manila trench (McCaffrey, 2008; Schellart and Rawlinson, 2013; Bletery et al., 2016).

The tsunami hazard assessments conducted in the Manila trench can be classified into two categories: the deterministic assessment based on single or several end-member scenarios (e.g., Huang et al., 2009; Liu et al., 2009; Wu and Huang, 2009; Okal et al., 2011; Qiu et al., 2019; Xie et al., 2019), and the seismic probabilistic tsunami hazard assessment (S-PTHA) which is based on historical events or enormous synthetic earthquake scenarios (e.g., Liu et al., 2007; Thio et al., 2007; Wen et al., 2011; Ren L et al., 2014; Li et al., 2016; Sepúlveda et al., 2019; Yuan et al., 2021). In the following sections, we will discuss these two categories respectively regarding the specification of model parameters, advantage, and disadvantage of the approaches. Meanwhile, we choose some typical studies as examples to demonstrate the tsunami characteristics triggered by megathrust earthquakes in the MSZ.

2.1 Deterministic tsunami hazard assessment

The deterministic approach often considers the end-members (i.e., worst-case scenarios) or a handful of credible fault models with specific fault parameters including earthquake magnitude and fault geometry (i.e., length, width, depth, strike angle, dip angle, and rake angle), etc. Such fault models (scenarios) are usually constrained by structural geology, geophysical survey, and geodetic measurements.

For example, the earlier worst-case scenario proposed by Megawati et al. (2009) suggests a full-rupture scenario that ruptures the entire Manila trench from 12.5°N to 23.5°N. By assuming a fully-coupled megathrust since 1560, this model yields an estimated moment magnitude of M_W9.3 (Figure 2a), by using the velocity measurements from the GNSS sites deployed along Luzon islands, Taiwan island and the islands between them. The estimated maximum slip deficit is ~40 m in north-western Luzon which corresponds to the fastest convergence rate (86–90 mm yr^{-1}) (Figure 2a) (Yu et al., 1999; Megawati et al., 2009). In fact, the geological structures of the MSZ in the north differ significantly from the south, whether the entire Manila megathrust could rupture as a whole in a single event or rupture partially in small piecemeals is still in active debate (Chen et al., 2014; Zhu et al., 2017; Gao et al., 2018). The megathrust develops a shallower dipping in the north than that in the south where it was affected by the subducting process of the Philippine trench in the east, resulting in a dual-subducting system. The northern segment of the MSZ is controlled by the subduction accretionary process, developing a large accretionary prism between the trench and the forearc region. In the central segment at 16.5°N, the seafloor develops a series of northeast-trending seamounts named Huangyan Dao Sea Mount Chain (Zhu et al., 2017). Whether the seafloor roughness raised by such seamount chain impedes seismic rupture propagation or acts as asperity remains elusive (Wang and Bilek, 2014; Bilek and Lay, 2018). Considering the spatial variety of the key features in the trench, including the structural difference between the northern and southern segments of megathrust, the spatial distribution of the coupling ratio on the fault, and tsunami excitation efficiency in the shallow accretionary wedge, Qiu et al. (2019) develop a series of possible rupture models. Qiu et al. (2019) implement the seamount chain as a boundary and divide the MSZ into three segments, i.e., the southern segment (14°−16°), the central segment (16°–19°), and the northern segment (19°–22°). The corresponding slip deficit of each segment is calculated by the coupling ratio and convergence rate from (Hsu et al., 2016), assuming a seismic return period of 1000 years. The cumulative strain of each segment is equivalent to moment magnitude M_W8.8–9.0 earthquakes (Qiu et al., 2019). In addition to these worst-case scenarios, many other rupture models were proposed to investigate the characteristics of tsunami waves and their associated impacts by considering earthquakes occurring at different locations, depths on the megathrust with variable moment magnitudes (e.g., Liu et al., 2009; Wu and Huang, 2009; Nguyen et al., 2014). For example, Liu et al. (2009) divided the "S-shaped" Manila trench into 6 segmented faults. The magnitudes of these segments were assumed as M_W8.0 with the fault dimensions and averaged slips being determined by the empirical scaling relationship (Wells and Coppersmith, 1994). Using a similar approach, Nguyen et al. (2014) specified 100 rupture scenarios with various magnitudes between M_W6.5 and M_W9.3 and different depths at 15, 30, and 55 km to assess the tsunami hazard along the coastline of Vietnam.

Among many of the deterministic scenarios, we select Megawati et al. (2009) and Qiu et al. (2019) as examples to demonstrate the hydrodynamic features of tsunamis and the

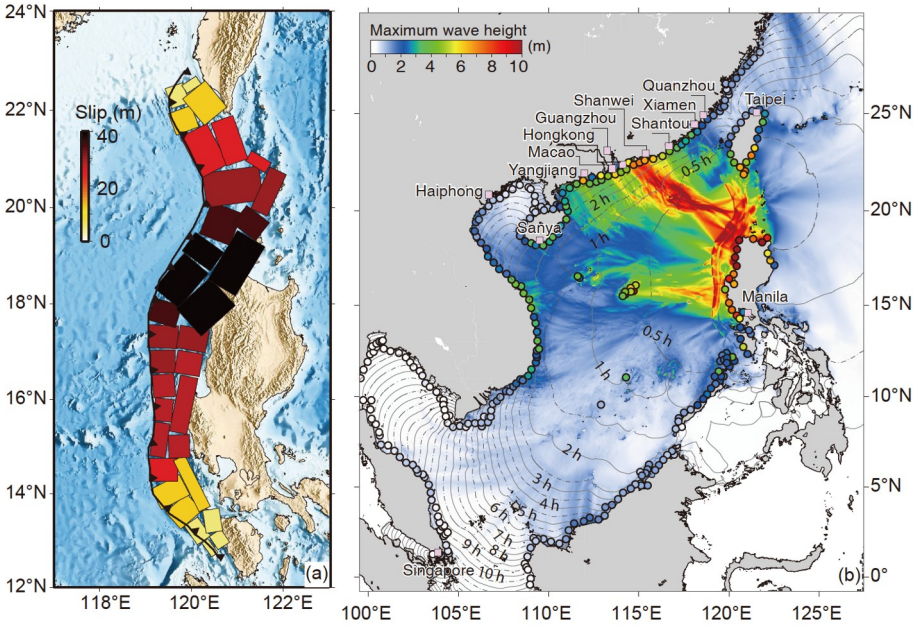

Figure 2 (a) The slip distribution of the end-member worst-case scenario proposed by Megawati et al. (2009); (b) The resultant maximum tsunami wave height and arriving time. Colored circles represent the wave height at 10-m water contour lines. The bathymetry data is retrieved from the 15 arc-second resolution grid of General Bathymetric Chart of Oceans (GBECO_2019).

hazard impact in the SCS region. We use tsunami software package COMCOT (Cornell Multi-grid Coupled Tsunami Model) (Liu et al., 1998; Wang and Power, 2011) to model wave propagation from the deep basin to coastal areas in the SCS. Nonlinear shallow water equations are applied to the whole simulation domain to better resolve the nonlinearity and bottom friction in the shallow water region. The modelling results are shown in Figures 2 and 3. With the coastal regions in Southern China as the main focus, we summarize the most important tsunami features in the following aspects: (1) Besides the coastlines of the southern Taiwan island and the western Luzon which are located in the near-source region, the southern coastline of China faces the greatest tsunami threat originated from great earthquakes in the MSZ (Figure 2). Most importantly, the GNSS observations suggest that the northern Luzon segment which poses the highest tsunami threat to the southern China has the highest convergence rate. Thus it has been accumulating the highest slip deficit. Tsunami waves generated by earthquakes in the offshore Luzon segment have a focused energy directing towards the coastal area in Guangdong province, especially in eastern Guangdong where the energized tsunami waves reach up to 4–10 m, as the result of the fault orientation and the bathymetric feature in the northern SCS (Figure 2b); (2) Simulation results of the segmented rupture models suggest islands in the SCS and the southern coastline of China would experience hazardous tsunami waves, regardless of the rupture locations. In particular, when rupture occurs in either the northern or central segments, the tsunami waves will focus their energy toward the southern coastline of China with the maximum wave energy distributed mainly along the coastal region of the Guangdong and Fujian province (Figure 3a, 3b). Note that when earthquakes happen in the central or southern segment, the Zhongsha and Xisha islands in the SCS will experience stronger hazard impact than ruptures in the north segment (Figure 3c); (3) as the result of the strong variation in bathymetry at the continental shelf in the northern SCS, the energy of tsunami waves focuses in several locations of the southern coast of China, including Yangjiang, Macao and Zhuhai in the western Pearl River and Shanwei from west to east . These regions would experience higher waves than their neighbouring coastlines, thus having a higher hazard potential than other regions (Figures 2b and 3); (4) tsunami waves could reach the Zhongsha and Xisha island in less than half an hour or one hour, respectively. Depending on the rupture location, the tsunami arrival times differ slightly. Tsunami waves initiated in the northern segment could arrive at eastern Guangdong province in 2–3 hours, earlier than that generated by the remaining segments. However, tsunamis initiated in the central and southern segment arrive at the Zhongsha and Xisha islands half an hour earlier than that initiated in the northern segment.

If a giant earthquake of M_W9.0 similar to the 2004 M_W9.1

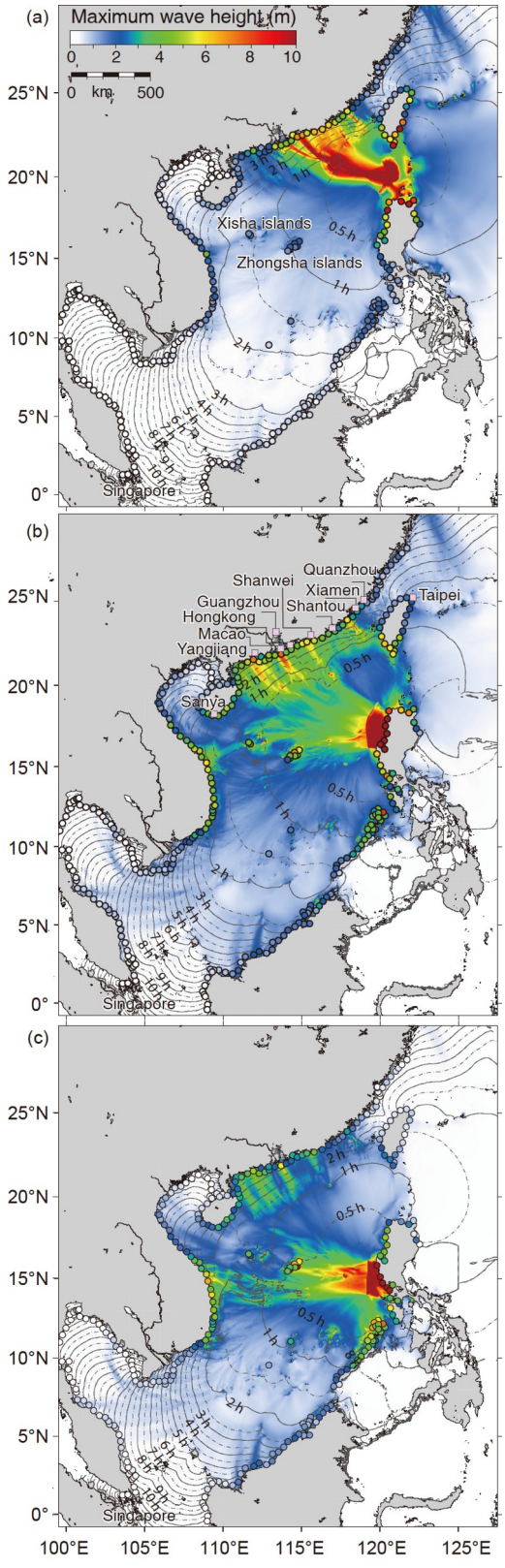

Figure 3 Maximum tsunami wave height prediction from the rupture models of Qiu et al. (2019). (a)–(c) present the maximum wave height and arriving time predicted by ruptures in the northern segment, the central, and the southern segment of the Manila subduction zone, respectively (model parameters setup is the same as that in Figure 2). The figure is modified from Qiu et al. (2019).

Sumatra-Andaman earthquake in the Indian Ocean or the 2011 M_W9.0 Tohoku-Oki earthquake in the Pacific ocean occurs in the SCS, the disastrous consequences are unimaginable. As the area of the SCS is only 350 km^2, which is 1/20 of the Indian Ocean (7056 km^2), and 1/50 of the Pacific Ocean (18134 km^2). The semi-enclosed nature of the SCS implies that the energized tsunami waves can only propagate and dissipate within the small basin without leaking into the surrounding oceans. Giant tsunami waves would distribute in the source region and along the path of wave propagation. Even when the waves dissipate to smaller amplitudes, they can also be reflected back and forth between the coastlines in the basin, leading to high-amplitude water oscillation that could sustain an ultra-long time period in the coastal regions. Such tsunami events had occurred in the Japan sea, which also features with the semi-enclosed setting similar to the SCS. The 1983 M_W7.9 Japan sea earthquake generated damaging tsunami waves that cause sea level fluctuation lasting for 2-days (Satake and Shimazaki, 1988). Based on the spectral analysis of recorded tsunami waveforms and numerical simulations, Satake and Shimazaki(1988) conclude that the ultra-long water level fluctuation is mainly caused by multi-reflection of the tsunami waves between coastlines within the semi-enclosed Japan sea. The multi-reflection caused the free oscillation of the water levels in the entire Japan sea. Even for the Pacific Ocean which has vast ocean size, basin-wide oscillations could also be excited by large earthquakes, as illustrated in the case of the 2011 Tohoku-Oki giant tsunami event (Heidarzadeh and Satake, 2014). Sea level oscillations induced by this tsunami sustained for 4–5 days in the Pacific Basin (Saito et al., 2013). In view of this phenomena, for the tsunami hazard generated by the earthquakes in the MSZ, besides the disastrous hazard caused by coastal inundation, we need to pay special attention to the long lasting tsunami oscillation generated by the multiple reflections between the coastlines and continental slope within the semi-enclosed SCS basin.

2.2 Probabilistic Tsunami Hazard Assessment (PTHA)

The tsunami hazard assessment based on deterministic approach only provides limited numbers of scenario-based results and does not provide the probability of the corresponding rupture scenarios. Therefore, the results have limited use for land-use planning and disaster prevention and mitigation. In contrast, the probabilistic approach can offer the probability of disaster level within different return periods (Mori et al., 2018; Behrens et al., 2021). The PTHA has been widely applied in many regions near subduction zones, e.g., the northeast Atlantic Ocean and the Mediterranean Sea by the joint effort from countries in the European Union (e.g., Sørensen et al., 2012; Gibbons et al., 2020; Basili et al., 2021), the SCS region (e.g., Liu et al., 2007; Wen et al., 2011; Li et al., 2016, 2018; Sepúlveda et al., 2021; Yuan et al., 2021), Japan subduction zone (Fukutani et al., 2014; Goda et al., 2015), US (e.g., González et al., 2009; Park and Cox, 2016), Java (e.g., Davies and Griffin, 2018), New Zealand (e.g., Mueller et al., 2015; Power et al., 2015) subduction zones.

The basic procedure of tsunami hazard assessment is borrowed from the Probabilistic Seismic Hazard Assessment, PSHA. PTHA is often carried out at synthetic wave gauges deployed at isobaths with certain water depth (e.g., 10 m/20 m/50 m) by simulating all the possible earthquake scenarios which could generate appreciable tsunami waves at these gauges. For each potential seismogenic zone, the Gutenberg-Richter relationship, namely earthquake frequency-magnitude, needs to be established in order to create a long-term (i.e., 100,000 years) earthquake catalog. Within the catalog, tsunamigenic earthquakes (e.g., $M_W \geq 6.5$) are randomly chosen (e.g., using a Monte Carlo method) to conduct a large number of tsunami simulations (e.g., 10^4–10^6). Then the database of maximum tsunami wave height can be developed at each synthetic wave gauge. To maximumly reduce the computational demand, the megathrust fault is discretized into many rectangular unit sources, on which Green's functions database is built. By using Green's functions database, the tsunami wave height at any synthetic wave gauge is determined by the linear superimposition of all Green's functions corresponding to different rupture locations and slip distributions. Finally, for any particular synthetic wave gauge, the probability of peak wave height can be quantified for different return periods or a specific time range.

The regional PTHA provides the relative hazard level at nearshore region which serves as the key reference for local PTHA. Local PTHA usually involves high-resolution simulations of coastal inundation in selected high-disastrous areas (Li et al., 2018). Different with the regional PTHA in which the maximum wave height at offshore synthetic wave gauges are the main output, the outputs of local PTHA include tsunami wave height, inundation depth, and flow velocity in the inland inundation areas. As a result, the simplified Green's functions approach becomes inappropriate. More complexed physical processes including the wave nonlinearity and bottom friction needs to be incorporated into the tsunami modeling when tsunami waves propagate into the shallow water region. Consequently, the full-life span of tsunami waves from generation, propagation to inland inundation processes need to be simulated for all the earthquake scenarios that can potentially cause inundations. To ensure the practicability of simulation results, the resolution of the topography needs to be in the order of 1–10 m which will significantly increase the computational burden (e.g., Volpe et al., 2019; Gibbons et al., 2020; Behrens et al., 2021).

In the procedure of PTHA, considerable uncertainties exist in the analysis, which include the physical characteristics of the earthquake source, hydrodynamics of the tsunami wave propagation and inland inundation process (Behrens et al., 2021). Among them, the earthquake sources have the largest uncertainty, which has been the research focus and yet the most challenging problem in the PTHA (Grezio et al., 2017; Behrens et al., 2021). The major uncertainties of the earthquake source come from the potential maximum magnitude, occurrence frequency, rupture extent and slip deficit distribution, etc. The common challenge for the whole research community is that the earthquake magnitude and frequency are poorly determined due to the insufficient historical records. The potential rupture extents and return periods of great or giant subduction earthquakes play a crucial role in tsunami hazard assessment (Behrens et al., 2021). The challenge exists not only in places where moderate to great historical earthquakes are missing or regions with relatively short historical records, such as the Manila trench, but also in the seismically active regions with more complete historical records. For instance, a typical example in the Japan trench, where the magnitude of the 2011 M_W9.0 "3.11" earthquake is way beyond of the expectations predicted by the historical earthquakes (Mori et al., 2018). In some innovative effort, the regional tectonic structures and seismogenic mechanisms are integrated for more comprehensive PTHA analysis, with focus on the complexity of earthquake rupture characteristics. For example, developing more realistic slip deficit models that can be more consistent with observations of local geological structures and characteristics of the previous earthquakes (Goda et al., 2015; Davies and Griffin, 2018). In addition to considering the structural complexity, heterogeneous slip rupture models (Geist, 2002; Mueller et al., 2015; Li et al., 2016), amplified tsunami excitation in the shallow portion of the megathrust (Murphy et al., 2016), and also depth-dependent changes in shear modular rigidity (Davies and Griffin, 2020) are incorporated in the tsunami sources. Additionally, the state-of-the-art PTHA research also focuses on more detailed description of tsunami wave propagation and inundation process e.g., implementation of high-resolution bathymetry and topography data (Goda and Song, 2016), the nonlinearity of waves in the shallow water region (Yuan et al., 2021), the astronomical tidal effect on tsunami waves (González et al., 2021), and the effect of rising sea-level on tsunami impacts (Li et al., 2018; Sepúlveda et al., 2021).

Due to the scarcity of great earthquake records and modern seismicity, the PTHA in the Manila trench is challenging. In addition to the incomplete seismicity records, the limited spatial and temporal GNSS measurements, especially the measurements in the shallow trench, result in a poor understanding of the seismogenic behaviours in the MSZ. The current status of the MSZ including the absence of great earthquakes, rapid convergence rate, and high coupling ratio suggests that the MSZ has a high potential for great earthquakes, although the magnitude, frequency, and rupture extent are largely uncertain. To take these uncertainties into account, Li et al. (2016) develop two sets of earthquake-frequency relationships by using the historical seismicity records (1973–2014) and constraints from geodetic measurements (convergence rate and coupling ratio) (Table 1). These two datasets differ significantly in the earthquake return periods. Taking the M_W8.0 earthquake as an example, the estimated return time period is 232 years based on the geodetic data, while the return period is 1043 years based on the seismicity records, leading to a 5 times difference (Table

Table 1 Seismic return period of earthquakes estimated in the Manila subduction zone[a)]

	Estimated from historical seismicity			Estimated from geodetic observation		
	Zone I	Zone II	Zone III	Zone I	Zone II	Zone III
M_w	a=5.97	a=4.96	a=6.20	a=5.45	a=5.74	a=5.96
	b=1.20	b=0.94	b=1.12	b=1.0	b=1.0	b=1.0
7.0	467	93	80	75	39	23
7.2	810	143	133	120	61	37
7.4	1406	220	223	190	97	58
7.6	2441	338	372	300	154	93
7.8	4238	521	623	476	244	147
8.0	7357	802	1042	755	387	232
8.2	12772	1235	1743	1196	614	368
8.4	22172	1901	2915	1895	973	584
8.6			4876			925
8.8			8157			1466
9.0			13644			2324

a) Zone I, Zone II, and Zone III correspond to the segments defined in Figure 4a and 4b

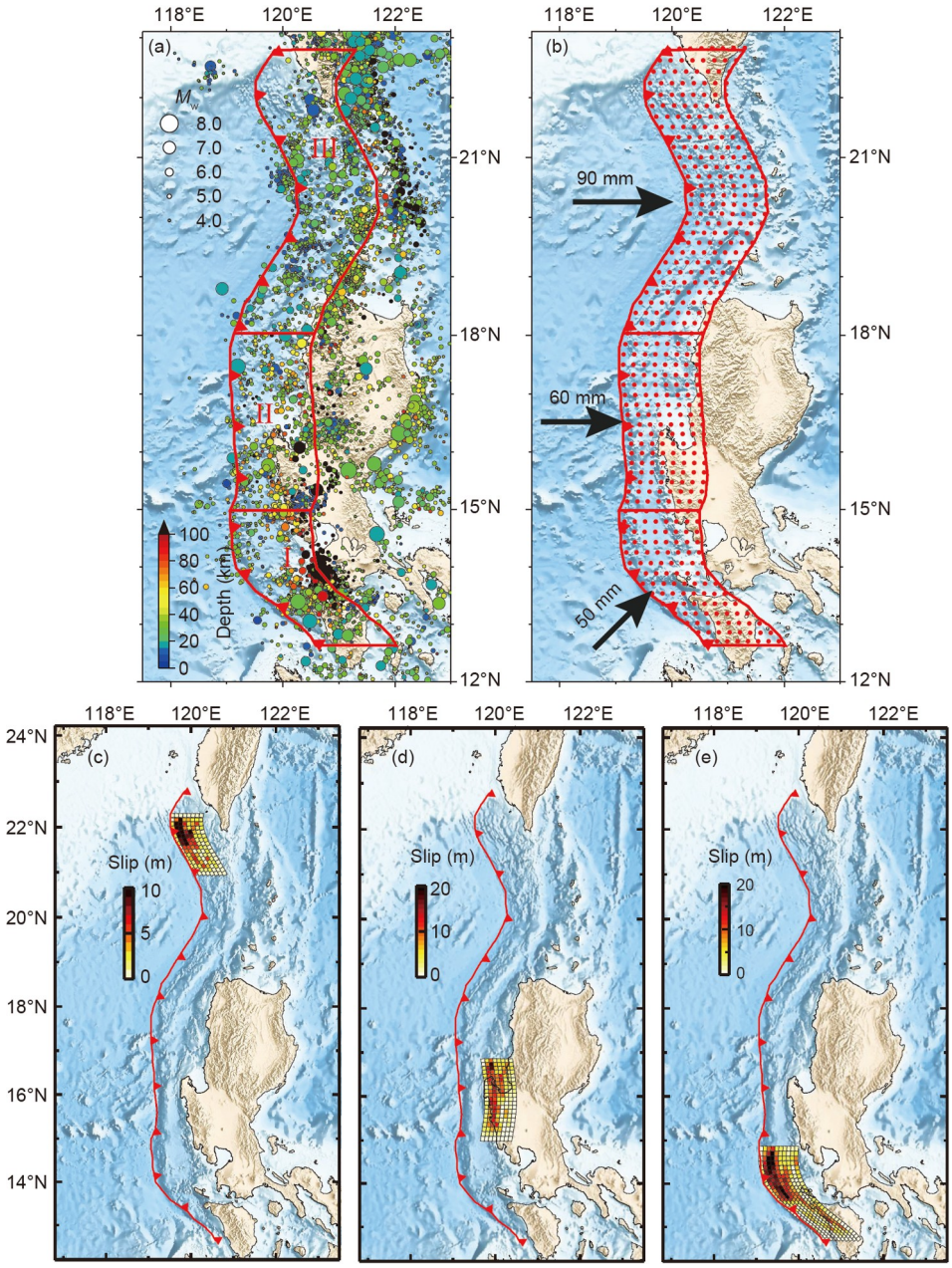

Figure 4 Fault segment and unit-slip element distribution in the Manila subduction zone. (a) Fault segments defined in the Manila subduction zone, (b) Unit-slip element source distribution, (c) a heterogeneous slip distribution example of M_W8.0 earthquake in the northern segment, (d) a heterogeneous slip distribution example of M_W8.2 earthquake in the central segment, (e) a heterogeneous slip distribution example of M_W8.4 earthquake in the southern segment. Figures are modified from Li et al. (2016, 2018).

1). To account for the possibility of these two datasets, Li et al. (2016) assigned 50% weighting to each of them for the final results.

Different from the traditional tsunami hazard assessment technique at that time, Li et al. (2016) introduced a novel approach by randomly selecting a rupture area on the megathrust where a heterogenous slip distribution is generated to compute the Green's functions. Such heterogenous slip distributions are expected to mimic the co-seismic slips more realistically, thus providing more reliable tsunami hazard assessment results (Figure 4c–4e). Recent studies have also assessed how the uncertainties associated with the maximum earthquake magnitude (Li H et al., 2017), earthquake frequency (Sepúlveda et al., 2019), and rising sea-level (Sepúlveda et al., 2021) affect the PTHA. Li H et al. (2017) conducted an analysis of the tapered Gutenberg-Richter relationships, which are determined by different approaches, including tectonic and seismic moment balance and occurrence of historical events. By comparing how the upper limit of the magnitude affects the PTHA results, they suggest the difference in magnitude upper-bound can lead to 2–6 times variations in the PTHA results. Sepúlveda et al.

(2019) proposed a Stochastic Reduced Order Model that can significantly reduce the numbers of earthquake scenarios in the Monte-Carlo simulation while still reasonably captures the uncertainty from the heterogeneous slip distribution. Under a non-static Poisson process framework, Sepúlveda et al. (2021) performed the PTHA analysis considering the effect of the global sea-level rise and concluded that the uncertainty raised by the sea-level change is comparable with that introduced by the earthquake occurrences.

In the following section, we take the study of Li et al. (2016) as an example to show the PTHA results in the SCS region with the megathrust earthquakes in the MSZ as the tsunami sources. The coastal regions between latitudes of 10°N–25°N, including the Philippines, China, and Vietnam face a larger tsunami impact than the remaining coastal areas (Figure 5). As expected, the near-source regions, e.g., the Philippines and southern Taiwan, China receive the worst tsunami hazard. It's worth to note that the southern coast of China, especially in Guangdong province would experience a comparable tsunami hazard level with the near-source region. In particular, in the coastal zone of the Guangdong province, the peak tsunami wave with 500-year return period reaches 1–2 m and could locally reach 2–3 m under favourable conditions; the wave can reach 2–3 m once in 1000 years, with some locations up to 5 m. Note that this hazard level is almost comparable with that in the near-source region like west Luzon. A detailed analysis about why the tsunami hazard level is surprisingly high is already mentioned in the previous section. We conclude with two main reasons: (1) the convergence rate of the western Luzon is the highest along the Manila trench as suggested by the long-term GNSS measurements, together with the coupling ratio estimates, this portion of the megathrust accumulates a huge slip deficit. Additionally, the tsunami energy path directly points toward the coastal region of the Guangdong province, especially in the coastline of eastern Guangdong. (2) The changes in wave directivity during tsunami propagation and the effect of the continental slope in the northern SCS. The maximum tsunami-wave energy is controlled by tsunami wave directivity and the characteristics of seafloor bathymetry along the propagation path. When an earthquake occurs, the generated tsunamis propagate along the direction perpendicular to the fault strike. During the propagation process from the deep ocean to the coastal area of southern China, tsunami waves are refracted as the result of shoaling effect due to the continental slope, eventually turning their direction perpendicular to the coastlines, towards Guangdong province.

When comparing the spatial distribution of the population density in and around the SCS with the tsunami hazard map, we notice that the places with high tsunami hazard levels coincide well with the populous areas. As one of the typical coastal flooding hazards, similar to the storm surge hazard, the tsunami hazard is strongly influenced by the local sea-level during the occurrence time. In the coastal zone of southern China, many places are characterized with low-lying topography, which are prone to disastrous hazards from extreme sea-level events. Under the effect of global warming, the sea level is rising rapidly, in this framework, both tsunami and storm surge are increasingly exacerbated. Take one of the representative city: Macao as an example, Li et al. (2018) upgrade the regional PTHA to the local coastal area and investigate the impact of sea level rise with 0.5, 1, and 1.5 m. They find that, with half meter sea level rise, the return period of the inner harbour of Macao Peninsula experiencing 1-meter tsunami wave reduces from 800 to 458 years (Li et al., 2018). This finding implies that in the context of sea-level rise as the result of global warming, the

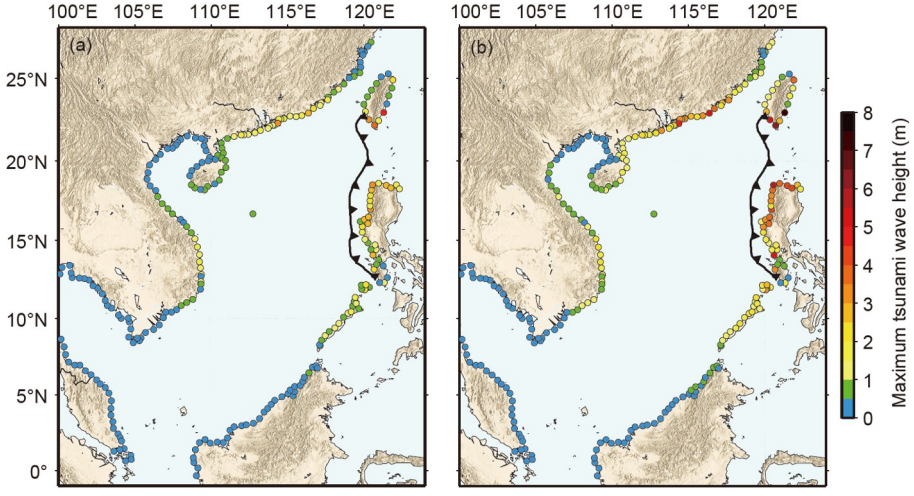

Figure 5 Tsunami hazard assessment in the SCS from megathrust earthquakes in the Manila subduction zone. (a) Maximum tsunami wave height distribution once in 500 years, (b) Maximum tsunami wave height distribution once in 1000 years. These observational locations are located along with the 10-m isobathic bathymetry. Figures are modified from Li et al. (2016).

possibility of the coastal area suffering the same level of tsunami hazard will be largely increased, therefore the coastal engineering protection facilities are needed to be upgraded or improved properly.

2.3 The challenges of tsunami hazard assessment in the MSZ

Although many studies have been conducted to assess the tsunami hazard using both deterministic and PTHA approaches in the MSZ, we must keep in mind that these results still remain largely uncertain. The uncertainties mainly come from lacking of great earthquake records and near-trench seafloor observations. Our understanding of the earthquake frequency, maximum earthquake magnitudes and rupture characteristics is still very limited (Yue et al., 2020). We summarize the major uncertainty in the tsunami hazard assessment as follows:

(1) Whether the Manila subduction zone rupture in segments or as a whole remains largely uncertain. Available geophysical data including multi-seismic reflection profiles, seismic profiles determined by OBS, and high-resolution bathymetry suggests that the geological structures in the northern and southern Manila trench differ dramatically (Chen, 2014; Zhu et al., 2017; Gao et al., 2018). Separated by the central seamount chain, the MSZ can be divided into the northern, central, and southern segments: the northern segment is controlled by the accretionary subduction process, which has developed a wide accretionary prism between the trench and the forearc basin; the southern segment is likely governed by the erosive subduction process and tectonic erosion process; while in the seamount chain area of the central segment where the seafloor bathymetry is complex, and roughness is high. Under the effect of both accretionary and erosive subduction processes, the central segment develops a much narrower accretionary prism (Zhu et al., 2013; Armada, 2016). The key question is whether the presence of subduction seamount can act as a barrier that impedes the rupture from propagating into the northern segment or an asperity that can promote rupture through or nucleate earthquake itself. Earthquakes with both mechanisms have occurred globally, indicating that both whole-trench-rupture and segmented rupture are possible (Taylor et al., 2008; Meltzner et al., 2012; Wang and Bilek, 2014; Philibosian and Meltzner, 2020).

(2) Enhanced tsunami excitation triggered by shallow megathrust earthquakes. In recent 20 years, many destructive tsunami events are observed at the global subduction zones, which were triggered by shallow ruptures in the trench. For example, the 2006 M_W8.3 Kuril (Ammon et al., 2008), the 2006 M_W7.8 Java (Fan et al., 2017), 2010 M_W7.8 Mentawai, western Sumatra (Hill et al., 2012), and the 2011 M_W9.0 Tohoku-Oki Japan "3·11" events (Wei et al., 2012). These events widely occurred in many subduction zones globally, We can classified these events into two categories: tsunami earthquake and trench-breaking ruptures (Lay, 2018; Geersen, 2019). These two classes differ in the seismic moment by two orders of magnitude, but a common characteristic of them is that they both rupture the shallow portion of the megathrust, and generate a similar order of the maximum runup, suggesting the shallow megathrust or outer wedge is the primary source responsible for the tsunami amplification. The occurrence of the shallow earthquakes challenges the widely accepted perception that the shallow megathrust beneath the accretionary sedimentary wedge is aseismic. In contrast, the shallow accretionary sedimentary wedge can accumulate strain energy and is capable of producing large earthquakes (Moore et al., 2007). The clay-rich sedimentary wedge is mechanically weak and has relatively low rigidity, thus the coseismic slip value is larger with the same seismic moment, and sometimes co-seismic weakening phenomenon occurs, which further lubricates the fault by slipping a huge distance, thereby amplifying tsunami waves (Bilek and Lay, 2018; Lay, 2018). The best example for a huge shallow slip event is the 2011 Tohoku-Oki earthquake and tsunami event. Solid evidence from the seafloor measurements show that the megathrust slipped by ~50 m in the trench, and generated a huge tsunami (Lay, 2018). In addition to the direct observation in the Japan trench, geological surveys in many subduction zones disclose that the outer wedges develop many complex high-angle imbricate thrust faults and fold structures. The fault-related structures are believed to be activated during several typical tsunami earthquakes and trench-breaking ruptures. Such structures can transfer the shallow megathrust slip to the high-angle thrust system in the outer wedge, therefore efficiently exciting the tsunami waves and producing unexpectedly larger tsunami impact (Moore et al., 2007; Hubbard et al., 2015; Fan et al., 2017; Hananto et al., 2020). The activities of outer wedges are poorly monitored as they are commonly located in the near-trench areas, which are usually far away from land-based geodetic observational systems. However, Yokota et al. (2016) and Gagnon et al. (2005) successfully captured the activity of the shallow megathrust by using the seafloor geodetic system. They conclude that the Nankai and Peru-Chilian subduction zones are highly coupled and have a large shallow slip deficit, highlighting that the shallow megathrust is capable of initiating damaging tsunami waves. In the Manila trench, the geological structure in the northern segment is strikingly similar to the fault system of the Nankai trench and several other subduction zones where great or giant earthquakes and tsunamis had occurred (Lin et al., 2009; Hubbard et al., 2015; Yang et al., 2020). Consequently, we should pay special attention to the tsunamigenic potential of the shallow megathrust.

(3) The spatial distribution of coupling ratio on the

megathrust remains poorly determined. The coupling ratio reflects the status of the strain accumulation during the convergence process, which is a crucial factor to assess regional potential earthquake and tsunami hazards. Yet, this ratio is largely unknown in the MSZ. Hsu et al. (2016) proposed two distinctive coupling models (A and B) by conducting a block modelling which is constrained by GNSS observation in Philippines and Taiwan, China between 1998 and 2015 (Figure 6). The major difference between A and B is that model B included the North Luzon Trough Fault (NLTF) in the block modelling. Model B yielded significantly higher coupling ratio estimates on the shallow megathrust between 17°N and 20°N which coincides with the source region responsible for tsunami excitation. Model A estimates a relatively low coupling ratio on the majority of the megathrust, while Model B yields a high, nearly 50%, coupling ratio. As limited by the spatial distribution of observational data, the estimated coupling ratio only covers the region between the latitudes of 14°N–20.5°N. The coupling ratios in the northern and southern segments are missing, therefore, the current status of cumulative strain cannot be quantified. Unfortunately, the northern segment of the MSZ is exactly the place which poses the largest tsunami threat to the southern coastline of China.

The uncertainties we summarized in this section affect the tsunami hazard assessment in various ways. For example, the tectonic setting and morphology structure of the seismogenic zone in the MSZ essentially define the earthquake nucleation mechanism; fault segmentation determines the maximum magnitude of earthquake; the coupling ratio defines the earthquake occurrence frequency. Neglecting the tsunami amplification effect of the shallow megathrust ruptures might result in a significant underestimation of tsunami hazard. These are the key factors that strongly affect the PTHA results (Li et al., 2016; Sepúlveda et al., 2019; Yuan et al., 2021). To minimize the effects associated with these uncertainties, we suggest the following future research directions: (1) Geologically, investigate the geological structure and rock properties of the shallow megathrust by drilling, coring, and logging, through ocean drilling program in the northern segment of the Manila megathrust. In addition, deploy seismometer and all sorts of sensors in the borehole to build up the seafloor observational system which can better monitor the earthquake activity, pore-fluid pressure, temperature and rock frictional properties in the fault zone, therefore, leading to a better understanding of the stress evolution changes and characteristics of the earthquake nucleation phase (Lin et al., 2017). (2) Seismologically, deploy broadband OBS to monitor long-term seismicity and improve the accuracy of earthquake locations, then achieve better constraints on the geometry of the subduction slab (Ren et al., 2020). Alternatively, conducting joint surveys

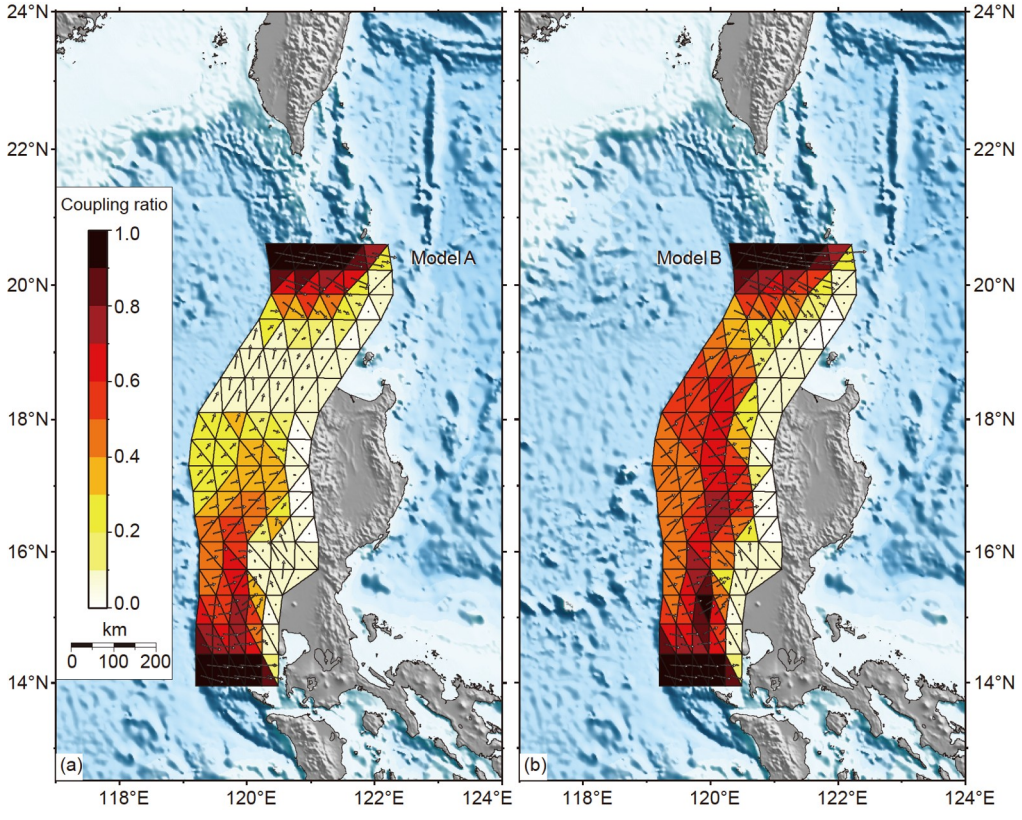

Figure 6 The spatial distributions of coupling ratio estimated from (a) model A and (b) model B on the Manila megathrust (modified from Hsu et al. (2016)).

through broadband OBS and 2D/3D deep seismic reflection to obtain high-resolution fault structures, especially the megathrust structure shallower than 50 km. Such data provides a scientific basis of the seismogenic mechanism and fault segmentation. (3) Geodetically, deploy seafloor GNSS to monitor the relative and absolute deformation in the northern segment of the Manila trench or incorporating the deformation monitoring instruments in the nodes of seafloor cable observation network to measure the slip rate of the megathrust. Such data allow us to quantify the coupling status of the trench and offer a crucial scientific basis for tsunami early warning and hazard assessment (Yokota et al., 2016). In summary, the assessment of earthquake activity and tsunami hazard requires constantly updated geophysical data, and calls for an integrated knowledge of seismology, geodesy, and ocean drilling etc. Seafloor deformation observations and geophysical surveys in the fault zone are the key approaches to study the kinematics relationship between the megathrust and the branching faults, as well as the slip rate and coupling ratio. All these efforts provide quantitative constraints on the seismics and tsunami hazard assessments.

3. Characteristics of the earthquake and tsunami in the LFZ

3.1 Tectonic structure features and historical earthquakes in the LFZ

Under the driven force of the complex subduction systems, the SCS regions have developed different tectonic elements. Among which, the zonation of the continent of Southern China and the continental shelf of northern SCS is very distinctive (Liu, 1981). The distinct zonation is also clearly reflected in the observational and survey data in gravity, magnetic anomaly, geomorphology, and satellite images etc (Zhong, 1987). Using these observations, Liu (1981), for the first time, defined this subarea as the LFZ. The LFZ connects Niushan island in the east and the Beibu Bay in the west, going through Nanri Island, Nanpeng Islands, Dangan Islands, etc at a water-depth ranging between 30 and 50 m in the continental shelf. The fault has the general orientation of NEE and extends more than 1000 km (Liu, 1981, 1985; Zhao et al., 2003; Xu et al., 2006). Previous studies (Xu et al., 2006; Cao et al., 2014) suggest that the tectonic stress that controls the development of the LFZ is strongly affected by the surrounding subduction zones and the evolution process of the SCS basin itself, behaving differently over a geological time scale. In particular, the tectonic stress was reversed during the transition time from Mesozoic to Cenozoic, which can be characterized as compressional stress, extensional stress, complex stress adjustment, and compression-shortening stress processes. Such complexed stress field forms the fault systems orientated in NE, NEE and NW directions (Liu, 1985; Yao, 1993; Cao et al., 2014; Xiong et al., 2018). These fault systems interact with each other and have developed a unique tectonic element in the continental margin of the northern SCS, generating a complicated tectonic stress field. This stress field controls the seismogenic behaviours of the LFZ and the associated tsunamigenic capacity in this region.

The LFZ is the most seismically active zone in northern SCS, which has generated 18 earthquakes with M>6 and 4 earthquakes with M>7 historically (Figure 7). Along this zone from west to east, the earthquakes with magnitude larger than $M\geq7$ include the 1605 M7.5 Qiongzhou, 1600 M7 Nan'ao, 1918 M7.5 Nan'ao and the 1604 M8.0 Quanzhou events (Chen and Huang, 1984; Sun et al., 2012). These earthquakes were all initiated at shallow focal depth with a thick sediment coverage in the continental margin, which are very destructive and caused huge casualties and property loss (Xu et al., 2006; Peng et al., 2017). Among them, the 1605 Qiongzhou (Xu, 2007) and the 1918 Nan'ao (Peng et al., 2017) are clearly accompanied with tsunami phenomenon. The source mechanisms of historical earthquakes occurring in the east portion of the LFZ such as the 1604 Quanzhou, 1600 and 1918 Nan'ao earthquakes, are most likely the right-lateral strike-slipping and thrusting mechanism (Peng et al., 2017). However, the focal mechanisms of historical events in the west portion such as the 1605 Qionghai earthquake, behaved as a right-lateral strike-slip and normal mechanism (Chen and Huang, 1989). In the Pearl river basin region, the central portion of the LFZ, no event with M_W>6 has been reported in historical records (Sun et al., 2012). Recently, on 1 Jan 2020, a M_W3.7 strike-slipping earthquake rattled this region. The striking angle of rupture surface is 78° which is consistent with the NEE orientation of the LFZ (Chen et al., 2021). The source mechanisms of these regional earthquakes suggest that the principal stress on the LFZ is orientated to northwest and southeast, but is modulated from east to west as the result of local tectonic structure and stress field.

In the eastern portion of the LFZ, affected by the subducting process of the Philippine plate, the stress field of the area between western Niushan Island and southern Penghu Islands is in shear and compression status (Xu et al., 2006). While in western LFZ, from western Leizhou to Qionghai region, the stress field is mainly in shear and extension status, as the result of complex tectonic activity between the Beibu Bay, southeastern of Qionghai basin and the Red-River fault (Chen and Huang, 1989). In the central portion of LFZ, the Pearl River mouth basin seats in the middle between the Philippine subduction zone (compression) to the east and the Red-River fault system in the west (extension) (Sun et al., 2012), in which the majority of earthquakes have a strike-slip faulting mechanism, while normal or thrust faulting mechanism is rarely observed (Chen et al., 2021).

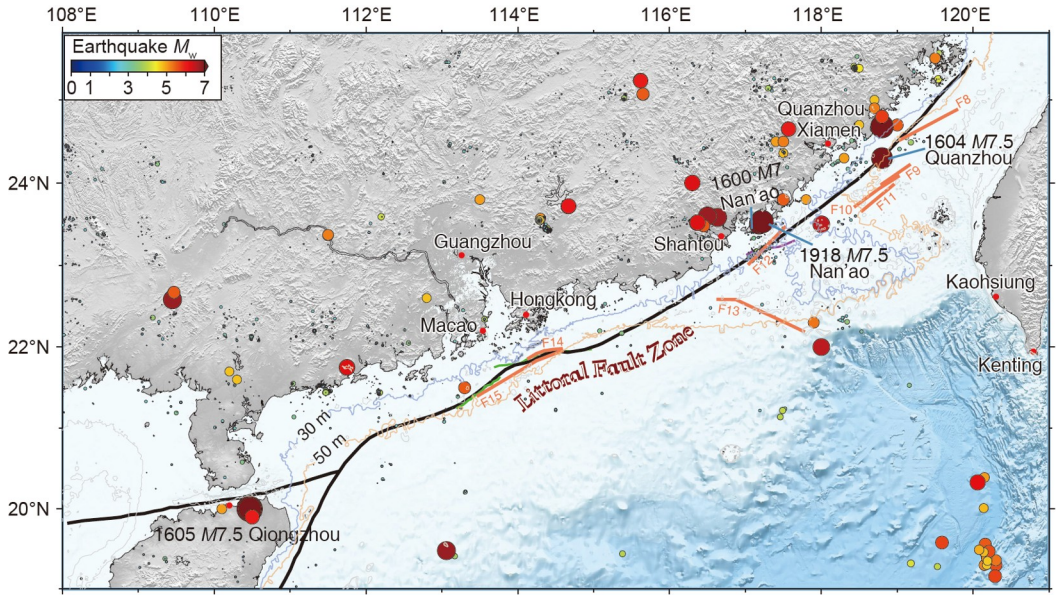

Figure 7 Historical and modern seismicity along the LFZ. The earthquake locations and magnitudes are from Cao et al. (2014), and the traces of F8-F15 faults are from Ren et al. (2016).

Recent micro-seismicity along the continental shelf in northern SCS can be grouped into 4 major regions. In particular, the southern Fujian-Eastern Guangdong, Yangjiang, Leiqiong are seismically very active, while the Pearl River Mouth Basin region is seismically quite characterized by sparse micro-seismicity (Sun et al., 2012). Different from the western and eastern of LFZ, the Dangan Islands segment of the LFZ in the offshore region of the Pearl River Delta has not ruptured by moderate or great earthquakes for a long time, and no earthquakes with M_W>6 occurred historically, forming a seismic gap (Sun et al., 2012). As it stays in the center area under a mixture of stress field from extension of basin area, compression from Philippine subduction zone in the east and extension from the Red-River fault in the west, this portion of LFZ segment may have a low slip deficit rate than that of the eastern and western fault segments, thus the seismic return period for a moderate or large earthquake is relatively longer. If this gap is indeed cumulating strain energy, large earthquakes could be expected.

The development in onshore-offshore seismic technology allows us to gain a more accurate and complete understanding of the fault structures from inland to oceanic (Zhao et al., 2003, 2004; Xu et al., 2006; Xia et al., 2012; Sun et al., 2012). The onshore-offshore seismic experiments in the LFZ reveal that the fault zone is about 6–10 km wide in the coastal area of southern Fujian to eastern Guangdong and Dangan Islands offshore the Pearl River Mouth basin. There is a lower velocity zone that starts at the seafloor dipping to southeast continuously extends to the Moho. Northwest of the fault zone, it is a typical continental crust within the subplate of southern China with a thickness of ~30 km; southeast of the fault zone, it is the thinned continental crust with thickness between ~25 and 28 km. A low velocity zone with a thickness of ~3–4 km is found located at the depth of 10–18 km within the lower crust. The thickness of this low velocity zone declines from the SCS basin to the continental margin in the northern basin and eventually vanishes at the LFZ (Xu et al., 2010; Cao et al., 2014). Further detailed studies of the relationship between seismicity and the fault structure suggest that seismicity often occurred at the boundary or in the transition zone between the low- and high-velocity zone that closes to the intersection of the conjugate fault system. For instance, the epicentre of the 1918 *M*7.5 Nan'ao earthquake (Xu et al., 2006; Xia et al., 2020) and locations of micro-seismicity in the Dangan Islands segment of the LFZ offshore the Pearl River Estuary (Xia et al., 2012). The presence of low-velocity zone in the crust is probably related to the partial melting under a high pressure and temperature thermal environment, which acts as a weak transition zone connecting the upper and lower crusts (Yang, 2003). It also plays a role in balancing and guiding stress, therefore transferring stress on fault or the conjugated NW fault branch. Once the stress concentrates in the weak zone at the fault intersections, sudden displacements could be triggered through seismicity (Shelley and Segall, 2000; Cao et al., 2014). Such dynamic process in the low-velocity zone most likely explains the rupture mechanism of the 1918 *M*7.5 Nan'ao earthquake (Xu et al., 2006). The complexed tectonic structures connecting the low-velocity zone and the conjugated fault system of the LFZ is recognized as the crucial stress-strain concentration regions in the northern continental shelf of the SCS region, thus is an important mechanic source for nucleating and developing large earthquakes (Xu et al., 2006, 2010; Cao et al., 2018).

3.2 Tsunami hazard assessment in the LFZ

The LFZ is located in the shallow water region whose depth ranges from 30 to 50 m. Consequently, attention is largely given to the associated seismic hazard rather than its tsunami hazard. Here we list several representative studies related to the tsunami hazard assessment in the LFZ region. Ren Y (2014) divide the LFZ into 8 potential tsunami sources (Figure 7), based on the seismic ground motion parameters zonation map of China (GB 18306-2015), as well as the regional geological structure, seismicity, and distribution of stress field. From east to west, the sources include the Quanzhou fault (F8), the Xiamen fault 1–3 (F9-F11), the Nan'ao fault (F12), the Taiwan fault (F13), the Zhu-Ao, and the Dangan faults (F14-F15). Among these faults, the eastern faults (F8-F12) are assigned with a maximum magnitude of M_W8.0, and the western faults (F13-F15) are assigned with a maximum magnitude of M_W7.5, which are implemented as the earthquake sources for the PTHA analysis in the SCS (Ren et al., 2016). Their results show that Hong Kong and Macao will have a probability of 5–10% to experience a peak tsunami wave up to 0.5 m within a 100-year return period, and such probability in Xiamen and Quanzhou is up to 30–40%. In Xiamen and Quanzhou, they will experience 1-meter tsunami wave once in 400–600 years. More recently, Yuan et al. (2021) implement the LFZ as the major tsunami source for the tsunami hazard assessment along the coastal region of China. It is important to point out that many features of the LFZ remains largely uncertain, e.g., the exact locations of the seismogenic zone, high-resolution fault geometries, potential maximum magnitude, seismic return period and focal mechanisms, etc. Unfortunately, these parameters are the crucial for assessing the potential hazards. For example, under the safety consideration, the majority of fault models are conservatively assumed as a thrust mechanism, yet in reality, previous analyses show that, from east to west of the LFZ, the focal mechanism changes from thrust faulting dominant to normal-faulting dominant. Different mechanisms generate dramatically disparity in tsunami magnitude, characteristics, and hazard level.

In this section, we take the 1918 Nan'ao earthquake as an example to demonstrate the hydrodynamic features of tsunami waves. Based on Li et al. (2022), we discuss how the focal mechanism of earthquakes influence their tsunamigenic capacity. Among all the recorded earthquakes in the LFZ, the 1918 M7.5 earthquake is one of few tsunamigenic events in the northern SCS. The tsunami phenomenon was clearly observed and documented along the coastlines of Guangdong and Fujian provinces after the earthquake. The "Compilation of Chinese historical earthquake data" mentions that "At 14:07 on 13 February of 1918 (the 7th year of the Republic of China, the third day of the new year in Lunar calendar), an earthquake with M7.3 occurred in Nan'ao region (23.60°N, 117.3°E) in Guangdong province. In Tong'an, Fujia province, the ground experienced strongly shaking, and the seawater receded before rose again, sank many ships. In Shantou, Guangdong province, a ship was moored in the harbour, but was stranded after the earthquake" (Xie and Cai, 1983). The phenomenon including "the seawater receded and rose again" and "ships were stranded after the earthquake" indicate that the coastal regions had experienced a leading-negative tsunami wave, most likely caused by the co-seismic subsidence during the earthquake. Constraint by this information and the latest geophysical data, Li et al. (2022) specified the 1918 Nan'ao earthquake parameters (i.e., epicenter, rupture extent, fault geometry), and conducted a series of tsunami simulations using various earthquake parameters. The simulated tsunami impacts suggest that the tsunami waves concentrate in the east and south of the Nan'ao island near the rupture area with the maximum wave height up to 3–4 m in the Qingao Bay of Nan'ao island. Tsunami impact is less severe in Dongshan county in Fujian province and Shantou in Guangdong province (Figure 8). The tsunami waves arrive at coastal region of Nan'ao and Shantou in half an hour, and the arrival times at Quanzhou, Hong Kong and Macao are about 3 and 4–5 hours, respectively (Figure 8). Limited by the shallow water depth between 30 and 50 m, earthquakes in the LFZ can only generate localized tsunamis, but the tsunami waves triggered in this region have two alarming features: (1) the broad continental shelf and the LFZ running parallelly to the coastline of southern China afford an efficient structure to trap the tsunami waves within the continental shelf, which allows the waves to be reflected back and forth between the coastlines and the edge of continental slopes. The shelf resonance induced wave oscillation could sustain more than ~48 hours long (Figure 9). (2) the rapid rise and fall of seawater could produce strong currents that can cause potential damages to the harbours, wharves, aquacultural zones and infrastructures in the southern coast of China. Meanwhile, large coastal earthquakes could trigger a hazard chain including ground shaking, slumps, landslides/submarine landslide and associated tsunamis, which deserves special attention.

Li et al. (2022) conduct the sensitivity analysis of the fault parameters of the 1918 Nan'ao event. They find that the tsunami impact is largely dependent on the fault geometry and focal mechanisms. The thrust earthquakes and normal-faulting earthquakes are more tsunamigenic than the earthquakes with strike-slipping mechanism (Figure 10). Compared with studies investigating inland fault activities, investigating the fault geometry and present activity of the LFZ is much more challenging since the faults are buried under seawater. However, the advantages of studying submarine faults is that the geological record could be better preserved than that of inland faults. A crucial scientific

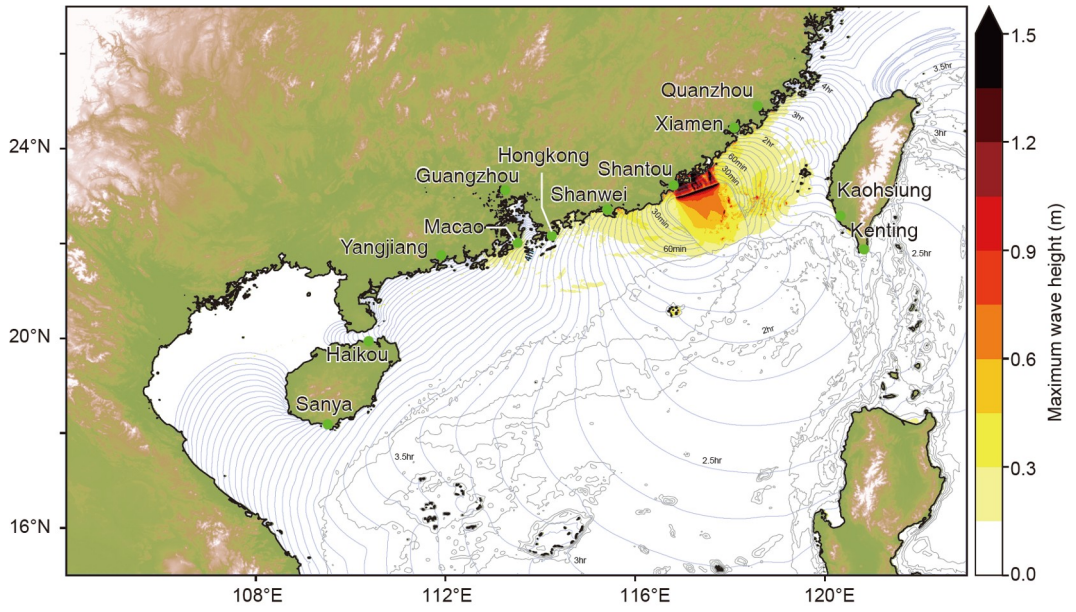

Figure 8 The distribution of maximum tsunami wave height overlaid by the contours of tsunami arrival time generated by the 1918 *M*7.5 Nan'ao earthquake. Colour scale is saturated at 1.5 m.

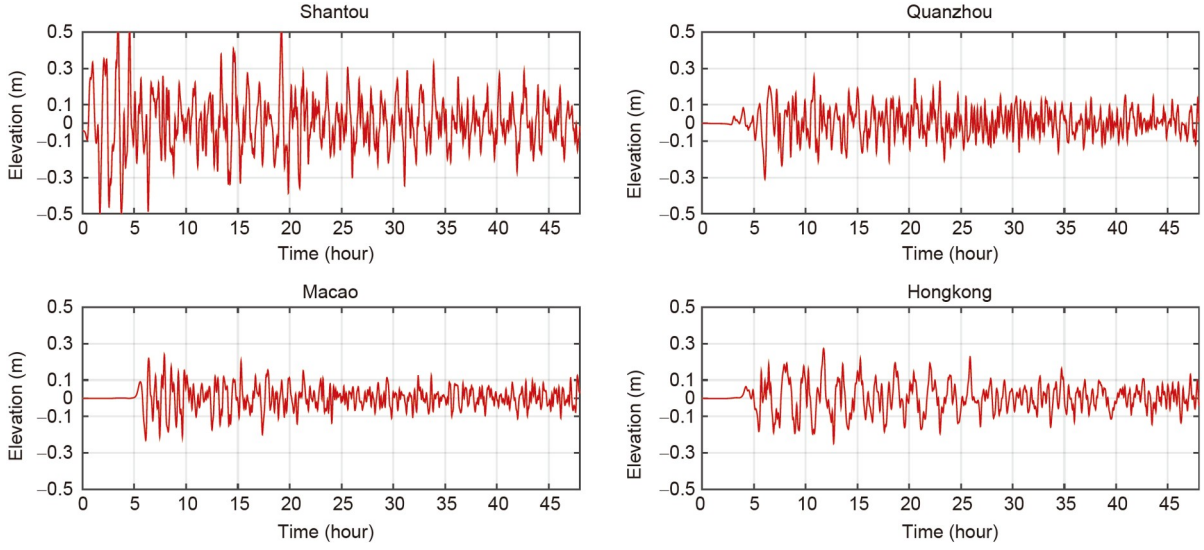

Figure 9 Time history of waves at typical locations in the SCS following the 1918 *M*7.5 earthquake tsunami. Figures are modified from Li et al. (2022).

question to be explored is how to investigate the activities of submarine faults through the relationship between the sedimentation and coseismic displacements and eventually uncovering the characteristics of large earthquakes. Integrated marine geophysical surveys are required to investigate the fault activities in the northern SCS, especially in regions with high seismic potential, e.g., the LFZ and active faults near the edge of northern continental slope. High-resolution 3D onshore-offshore seismic experiments and seafloor geodetic measurements are important tools to better understand the seismogenic behaviors, together with the detailed structure of the active oceanic faults. A comprehensive understanding of the characteristics of fault activities, segmentation, and seismogenic mechanisms is the scientific basis for seismic and tsunami hazard assessment in the northern SCS.

4. Submarine landslides and the potential hazard

4.1 The spatial distribution of submarine landslides in the SCS and analysis of historical events

Chen et al. (2007) have pointed out that large-scale submarine landslides in the SCS region are one of the potential

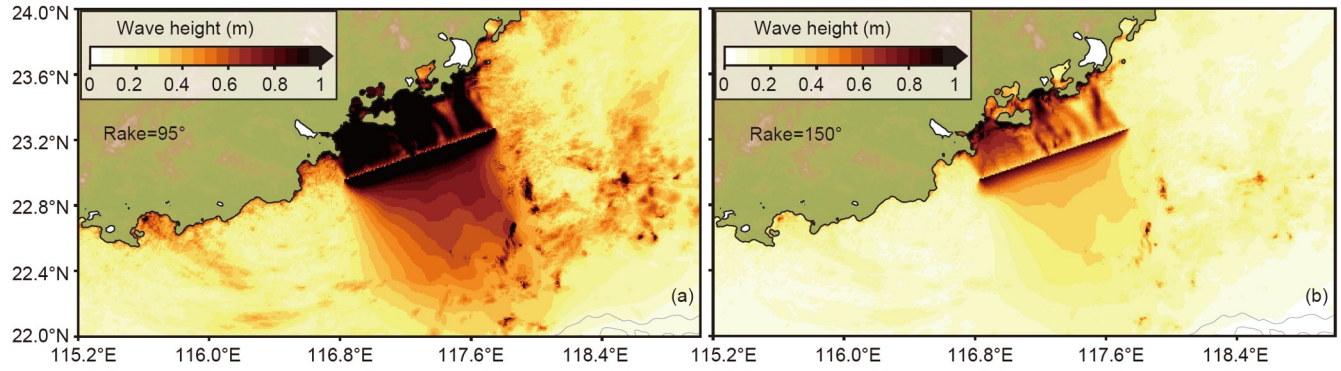

Figure 10 Comparison of the maximum tsunami wave height generated by earthquakes with different rake angles. The dip angle and strike angle are 75° and 70°, respectively for both models. Figures are modified from Li et al. (2022).

tsunami sources more than a decade ago when seafloor geophysical surveys are relatively scarce. With the increase in submarine explorations, numerous submarine landslides, particularly in the continental slopes, are identified through multi-beam bathymetric data and high-resolution seismic data (Figure 1). The volumes and numbers vary significantly in different continental slopes. Most of the landslide regions contain geological evidence of repeated paleo-slide records (Sun et al., 2018a; Wang et al., 2018). Among all the identified landslides so far, large-scale landslides are most densely distributed in the northern slope (Wang et al., 2018; Wu et al., 2018, 2019), which includes the Qiongbei slide in the Qiongdongnan basin (Li W et al., 2015), the Huaguang slide (Wang et al., 2013), the Baiyun slide complex in the Zhujiangkou Basin (e.g., Li W et al., 2014a, 2014b; Sun et al., 2017, 2018a, 2018b; Wu et al., 2011) and the Jiulong slide in the Taixinan basin (Wu et al., 2011). For the small to medium-scale landslides in the northern SCS, a few studies have investigated the landslides located in the Shenhu Canyon (He et al., 2014; Zhou et al., 2018; Wu et al., 2019). In the south, a giant slide (the Brunei slide) is reported in the continental slope between the Baram delta and the Nansha Trough (Gee et al., 2007; Ren et al., 2021). Influenced by the tectonic activities, the continental slopes are steeper in the west near Vietnam and in the east near the Philippines. Landslides in these regions are featured with large numbers but small volumes due to the limited accommodation space (Armada, 2016). Besides the landslides in the continental slopes, a large number of landslides are also revealed in areas surrounding the carbonate platforms in the SCS basin (Wang et al., 2018), e.g., typically, the Yongxing slide near the Xisha island (Li X et al., 2017) and the slumps in the Zhongsha island (Huang et al., 2020). The existence of a large number of landslides highlights the urgency of conducting a quantitative hazard assessment of landslide tsunamis in the SCS region.

Submarine landslides could cause direct damage to infrastructures located in the deep sea or seafloor, e.g., submarine cables, oil platforms, and pipelines (Fine et al., 2005; Hsu et al., 2008). Strong disturbance produced by the landslide movement could also induce localized but damaging tsunami waves, threatening the coastal region (Løvholt et al., 2019; McSaveney et al., 2000). The most typical example includes the M_W7.0 Pingtung earthquake doublet on December 26th, 2006, which triggered submarine landslides and turbidity currents in offshore southwest Taiwan, China. The submarine landslides and turbidity currents with the current speed of ~3.7–20 m s^{-1} broke nearly 20 submarine cables across the Kaoping Canyon and Manila trench, causing major failures in international telecommunication in the Southeast and East Asia (Hsu et al., 2008; Su et al., 2012). The Grand Banks earthquake and tsunami on 18th, November 1929 is another typical example demonstrating the damaging power of submarine landslides. The landslides broke 12 telegraph cables connecting the North America and Europe (Fine et al., 2005).

Historically, there are several tsunami events inside the SCS region which might involve the contribution of submarine landslides: the tsunami event occurred in the southern Hainan island on January 4, 1992 (Ren et al., 2019; Yu et al., 2020) and the 1781 tsunami event in the southwest of Taiwan island (Li L et al., 2015). The 1992 tsunami event was associated with a M_W3.7 earthquake in the offshore area of southern Hainan. After the earthquake, tsunami waves with an amplitude of 78 cm were recorded by a tide gauge (Yulin station) in the southern coast of Hainan island (Yu et al., 2016). This is the first instrumentally recorded tsunami event in the northern SCS. Since the magnitude of the earthquake is unproportionally small compared with the typical magnitudes of so-called tsunamigenic earthquakes, the earthquake-triggered submarine landslides are suspected as the main source for the tsunami (Ren et al., 2019). The Tainan event that occurred in the late 18th century is the most deadly tsunami event recorded in the SCS which are reported in the literature by different languages: English (Mallet, 1854), French (Perrey, 1862) and Chinese (Chen, 1830). According

to the report in the Chinese literature: Taiwan Interview Catalogue "In around the 4th and 5th month, 46th Qianlong year, the weather was fine. Suddenly the sea roared like thunder. Giant waves appeared. The water rose for tens of zhang high (1 zhang approx. equals 3+1/3 m). Villagers nearby were all submerged…": this description eliminates a typhoon-induced storm surge as the causative event. The French document reported that this event affected three principal cities and 20 villages, leaving thousands of people perished (see the detailed translation in the supporting information of Li L et al. (2015). Despite consistent reports from southwest Taiwan island, no corroborative information exists for neighbouring shorelines in southeast China or northwest Luzon island, Philippines, and a plausible source of this tsunami was mysterious. With the constraint from the documented tsunami impact, fault structure of the Manila trench and tectonic settings in southwest offshore Taiwan island, Li L et al. (2015) investigated tsunami characteristics generated by different sources (earthquake, volcano and submarine landslides) using numerical models. They suggest that the most likely source of this major tsunami event is a seismically-triggered submarine landslide (Li L et al., 2015). Considering the tectonic setting of southern Taiwan island, which features as steep continental slopes with complex submarine canyons, it is not unexpected that submarine landslides could have contributed to this tsunami event. In fact, landslide tsunamis triggered by moderate earthquakes have occurred worldwide, e.g., the July 17, 1998 Papua New Guinea (PNG) landslide tsunami event (Synolakis et al., 2002; Tappin et al., 2001) and the 2018 Palu earthquake and tsunami event (Liu et al., 2020; Schambach et al., 2021). With active faults up to thousands of kilometres developed along the nearshore and continental edge in the northern SCS, close attention should be given to the submarine landslides in the northern continental slope and the associated disaster chain. Submarine landslides are commonly located in continental slopes or near the islands which in most cases are closer to the target coastlines. Their unpredictable nature and limited arrival time challenge the current tsunami warning system. Quantifying the potential tsunami impact (e.g., tsunami arrival time, wave amplitude and inundation extent) generated by those landslides, therefore, becomes the primary approach to prepare the coastal communities.

4.2 Landslide tsunami hazard assessment in the SCS

Similar to the tsunami hazard assessment of seismic sources, tsunami hazards from submarine landslides can also be assessed through deterministic and probabilistic approaches. The tsunami generation mechanism of landslides is much more complex than earthquakes. The tsunamigenic capacity is determined by various kinds of factors, e.g., initial water depth (Fine et al., 2003; Li et al., 2019), landslide dynamics (sliding, slump, debris flow and turbidity flow etc.) (Zengaffinen et al., 2020), sliding speed and acceleration (Harbitz et al., 2014), landslide material and rheological behavior, etc. (Løvholt et al., 2015, 2017; Schambach et al., 2018; Kim et al., 2019). So far, the assessment of landslide tsunami hazards heavily relies on the numerical modelling of fluid dynamics. The procedure commonly starts with reconstructing the initial spatial distribution of landslides from the available geophysical and geotechnical data, including 2D/3D seismic data, multi-beam bathymetric data and sediment cores. The landslide dynamics are then simulated (Kim et al., 2019; Li et al., 2019) by treating the landslide material as a rigid slump (Enet and Grilli, 2007), viscous mudflow (Grilli et al., 2017; Ren et al., 2019), granular flow or multiphase flow (Si et al., 2018; Shi et al., 2019; Zhang et al., 2021a, 2021b). The initial surface elevation is generated by considering the interaction between the dynamic sliding process and the upper water layer. For the tsunami propagation and inundation process in a larger domain, numerical models based on nonlinear shallow water equations (e.g., COMCOT, GEOCLAW) or Boussinesq type equations (e.g., FUNWAVE, COULWAVE) are commonly applied (Geist and Lynett, 2014; Løvholt et al., 2020; Behrens et al., 2021).

Several studies have assessed the potential tsunami impact from several representative submarine landslides in the SCS using the scenario-based approach, including the Baiyun slide (Sun and Huang, 2014; Li et al., 2019; Ren et al., 2019; Sun and Leslie, 2020), the Brunei slide (Tan et al., 2017; Ren et al., 2018) and the landslides in the offshore Taiwan island (Li L et al., 2015), etc. Taking the Baiyun slide as an example, the landslide materials are treated as rigid slump (Sun and Huang, 2014; Sun and Leslie, 2020), viscous mudflow (Li et al., 2019) and mudflow based on Herschel-Bulkley rheological theory (Ren et al., 2019). Although these simulations used different landslide materials, volumes, and initial distributions, the results all indicate the tsunami hazard posed by submarine landslides is nonnegligible.

Here we demonstrate the potential tsunami impact of two giant landslides in the SCS: the Baiyun slide and the Zengmuansha slide (the Brunei slide). Both slides are located in the open continental slopes which contain geological evidence of previously repeated landslides (Gee et al., 2007; Sun et al., 2018b). Interestingly, based on the high-resolution seismic and bathymetric data, we find the two slides have comparable sizes with the estimated volumes of 1035 km^3 for Baiyun slide versus 1200 km^3 for Brunei slide and areas of 5500 km^2 versus 5300 km^2 (Gee et al., 2007; Sun et al., 2018a; Ren et al., 2021) (Figure 11). We investigate the sliding dynamics and their tsunamigenic capacity by applying the combined modelling approach NHWAVE (Ma et al., 2012) and FUNWAVE-TVD (Shi et al., 2012), treating the slides as translational mudflow. The Brunei slide could

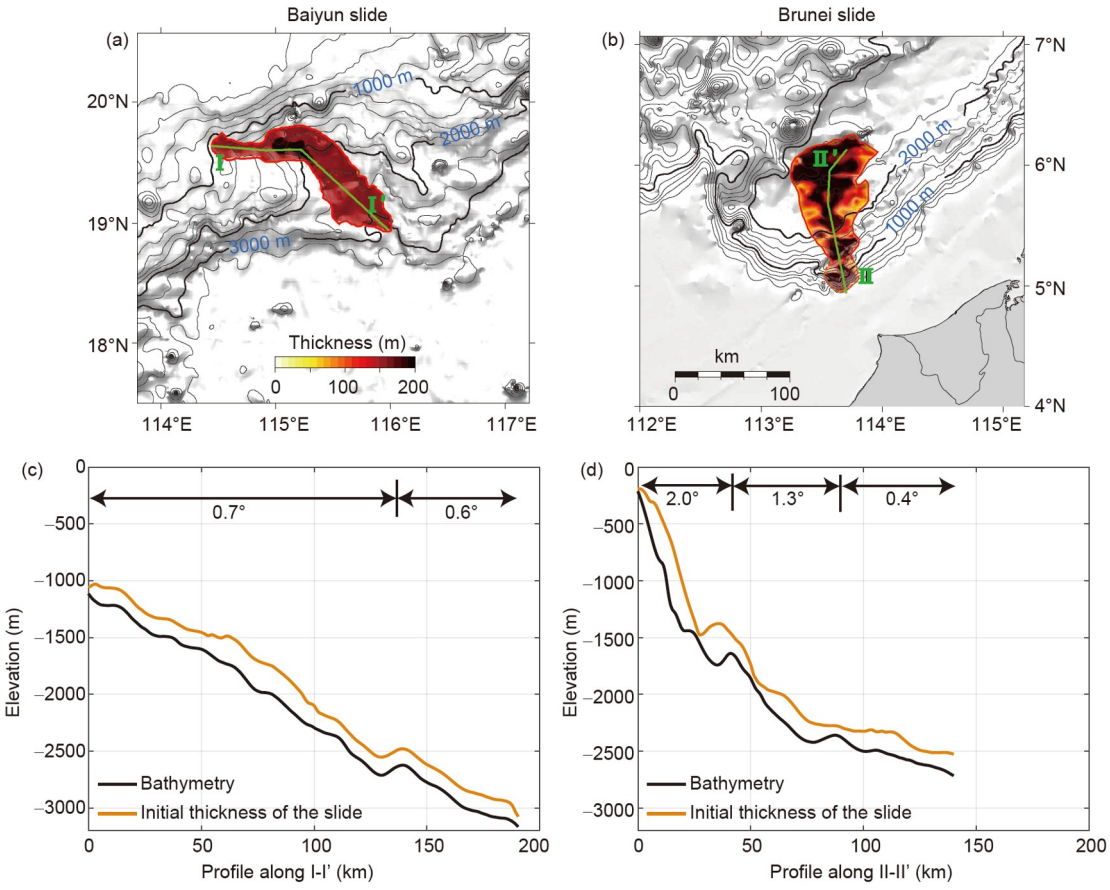

Figure 11 The initial distributions of landslide thickness of (a) the Baiyun slide and (b) the Zengmuansha (Brunei) slide. The slope and initial thickness along (c) transects I-I′ and d) II-II′.

generate significantly larger tsunami waves than the Baiyun slide despite that their sizes are similar (Figure 12). The key factors determining the difference are the steepness of the slope and the initial water depth of the slides. The Baiyun slide covers the water depth between ~1000 and 3000 m with an average slope of 0.6°–0.7°, while the initial water depth of the Brunei slide is shallower (200–2500 m). The slope near the head of the slide is ~2.6° and slowly becomes gentler from 1.3° to 0.4° (Figure 11c and 11d). The slope of the landslide source region is one of the key parameters determining the initial acceleration and sliding velocity of landslide. The initial water depths of landslides affect their efficiency of tsunami generation. When the sliding velocity is comparable with the propagation speed of tsunami waves, the wave could reach the peak due to the superposition of resonance (Fine et al., 2003; Yavari-Ramshe and Ataie-Ashtiani, 2019).

The results suggest that giant submarine landslides may cause damaging effects in the following aspects: (1) infrastructures located in the seafloor could be destroyed by the high-speed sliding material. Compared with the inland landslides, the spatial coverages of submarine landslides are significantly larger, up to thousands of square kilometres. With a sliding speed of 20–35 m s^{-1}, the moving landslide materials are powerful enough to break submarine cables and the foundations of ocean platform (Li et al., 2019); (2) Ocean engineering could be affected by the huge tsunami waves right above the source area. During the sliding process, tsunami waves could reach tens of meters (e.g., 8–15 m for the Baiyun slide) in regions above the source area, covering tens or hundreds of square kilometres. Oil platforms near the Shenhu Canyon or other ocean engineering facilities within this range could be affected by the hazardous waves (Figure 12); (3) Tsunami waves generated by the Baiyun slide could cause devastating damage to the densely populated Greater Bay Area. The wave focusing phenomenon in front of the Greater Bay Area shown in the earthquake scenarios is more pronounced in the scenarios with landslide sources. We attribute this focusing phenomenon to the unique bathymetric features and tsunami directivity effect. In the southern SCS, if landslides with volumes similar to the Zengmuansha (Brunei) slide occur, tsunami waves with localized wave heights of ~10–20 m could arrive at the Nansha islands in 0.5–1.0 hours, resulting in catastrophic effect (Figure 12).

PTHA is lagging behind for landslide sources (L-PTHA) compared with seismic sources (S-PTHA), especially in the

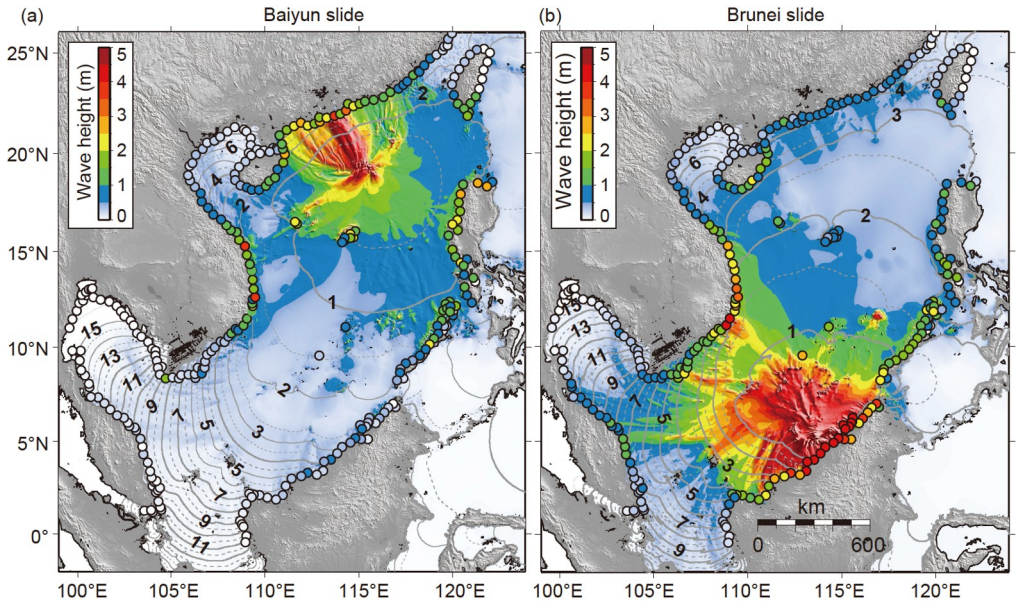

Figure 12 The maximum tsunami wave height generated by the Baiyun slide (a) and the Zengmuansha (Brunei) slide (b). The contours of tsunami arrival time are overlaid on the map.

SCS region. Although the scenario-based approach is still the main method worldwide (e.g., Geist et al., 2009; Leslie and Mann, 2016; Grilli et al., 2017; Li et al., 2019), L-PTHA is applied in regions with relatively rich geological and geotechnical data, e.g., the east coast of the United States (Grilli et al., 2009; Geist and Parsons, 2010; ten Brink et al., 2014), the Gulf of Mexico (Pampell-Manis et al., 2016), Canada (Leonard et al., 2014), New Zealand (Mueller et al., 2016; Lane et al., 2017) and the Mediterranean (Grezio et al., 2012, 2020), etc. Many assessments apply Monte Carlo simulation as the core algorithm. The first step is to establish the relationships among landslide numbers, areas, volumes and thicknesses according to the available landslide database. The relationships are commonly determined by their tectonic settings (ten Brink et al., 2006, 2014; Urgeles and Camerlenghi, 2013). The regions with landslide potential are then divided into different zones. For each zone, random landslide events can be generated based on the relationships established in the previous step using Monte Carlo simulation. The final step is to conduct tsunami simulations for each landslide event and assess the tsunami impact in the nearshore (Grilli et al., 2009; Pampell-Manis et al., 2016). Some processes involve simplified assumptions, for example, using the earthquake frequency as an important constraint on the recurrence interval of landslides (ten Brink et al., 2009), obtaining the estimated tsunami wave heights by applying the theoretical equations of long waves to idealized continental slope instead of modelling all the tsunami events (Grilli et al., 2009).

L-PTHA is very challenging due to several factors: (1) The temporal and spatial distributions of landslides are scarce in most regions. The majority of submarine landslides identified so far lack reliable occurrence times (Grezio et al., 2017). The recurrence interval of large-scale landslides could be several thousand years or even longer (Urgeles and Camerlenghi, 2013; Urlaub et al., 2013; Pope et al., 2015); (2) The tsunamigenic mechanism of landslide is very complex and diverse. Factors including landslide material, volumes, initial distribution, sliding speed/acceleration and rheological property all affect tsunami genesis. The complexity in the tsunami genesis and propagation process lead to great uncertainties in L-PTHA (Løvholt et al., 2020; Behrens et al., 2021). Despite great efforts have been made to obtain the spatial and temporal distribution of submarine landslides in the SCS region (Wang et al., 2018), challenges exist as the characteristics of submarine landslides developed in the different tectonic environments (submarine canyons or open continental slopes) are diverse in terms of their volumes and typical material (carbonate, viscous/non-viscous), thus differing in triggering mechanisms and landslide dynamics. For example, the landslides identified in the western continental slope near Vietnam are numerous but all with relatively small volumes due to the limited accommodation space. Before the L-PTHA could be more reliably conducted, more detailed landslide parameters are required, e.g., frequency-magnitude distribution and key geometrical features like volume, length, width, thickness, initial water depth and slope, etc. The focus of future research should include establishing the relationship between the peak ground acceleration associated with earthquakes from the active faults in the northern SCS and triggering criteria of landslide, the effect of natural gas hydrate decomposition and landslide instability, etc.

5. Paleo-tsunami deposits in the SCS

The big challenge of tsunami hazard assessment in the SCS is to answer whether this region has experienced large-scale tsunami events and what's the frequency of hazardous events. Taking the seismic activity of the global subduction zones as an example, the recurrence of large earthquakes and their associated tsunami event is usually in the scale of hundreds of or even thousands of years long (Satake and Atwater, 2007; Sieh et al., 2008; Philibosian and Meltzner, 2020). Such long return periods challenge the majority of coastal regions which only have scarce historical documents.

Historically, 58 tsunami events with different levels of validity are reported in the northeastern SCS (Lau et al., 2010) (Figure 1). Philippine Institute of Volcanology and Seismology (PHIVOLCS) documented 41 tsunami events with high creditability during 1589–2012 (Bautista et al., 2012). Vu and Nguyen (2008) reported 5 suspected tsunami events along the Vietnamese coast. Paris et al. (2014) collected 39 tsunami events with volcanic origin in Southeast Asia. The spatial distribution of these historical events suggests that most of the events surround Taiwan, China (Lau et al., 2010) and the Philippines (Bautista et al., 2012), especially in the eastern coast of these regions which are exposed to the circum-Pacific subduction zones. Few tsunami events are reported along the coasts inside the SCS. The most damaging event is the 1781 tsunami event which occurred in Tainan and Kaohsiung with tsunami wave heights up to tens of Zhang (an ancient unit used in China, 1 Zhang=3.33 m). The death toll is probably up to 40,000–50,000, according to different literature. Other events associated with possible tsunami phenomena include the 1076 "the sea surge" event in Chaozhou, Guangdong, the 1604 Quanzhou earthquake in Fujian, the 1605 Qiongzhou earthquake in Hainan (Xu, 2007), the 1918 Nan'ao earthquake in Guangdong (Peng et al., 2017) and the 1992 Hainan tsunami event (Yu et al., 2016). Moderate tsunami events with 1–2 m tsunami waves are also reported in the western offshore Luzon island of the Philippines (Figure 1). The source earthquakes responsible for these tsunami events include the 1983 M_S6.5 earthquake, the 1934 M_S7.6 earthquake, the 1924 M_S7.0 earthquake, the 1999 M_S6.8 earthquake and the 1828 M_S6.6 earthquake from north to south (Bautista et al., 2012). The historical documents are very limited in Vietnam due to historical reasons. Vu and Nguyen (2008) reported 5 suspected tsunami events that occurred in the years of 1877, 1882, late 19th and early 20th century, 1923 and 1978. Among all these events, a field survey suggests the tsunami wave may have reached 18 m high during the 1882 event. Considering the limitation of observational instruments during historical time, various classification and preservation of historical documents in different countries, the validity of existing tsunami records in the SCS region still varies considerably. The events recorded after the year of 1589 in the Philippines and 1604 in China are relatively more reliable.

Besides the historical documents, the only effective approach of reconstructing longer tsunami records is to rely on the paleo-seismic and paleo-tsunami records (Qiu et al., 2009; Yang et al., 2021). Tsunami deposits are the physical traces left behind by tsunamis when they propagate to the shallow sea and carry nearshore sediments, boulders and microbes inland. These deposits can be preserved in the geologic record in favourable conditions (Paris et al., 2010; Goff et al., 2011; Goto et al., 2012; Richmond et al., 2012). By using various proxies (e.g., inland sediment deposits, boulders, microbes, nearshore deposits and turbidite deposits) and interdisciplinary approaches (e.g., geological, geophysical, geochemical and sedimentological data), researchers reconstructed the recurrence of large earthquakes and tsunami events along the subduction zones of the Sumatra-Andaman (Jankaew et al., 2008; Meltzner et al., 2010; Maselli et al., 2020), Cascadia in north America (Satake et al., 2003; Atwater et al., 2005; Kelsey et al., 2005), Kuril Trench (Nanayama et al., 2003, 2007; Satake et al., 2005) and Chilean Trench in south America (Cisternas et al., 2005), etc. The physical property and spatial distribution of sediment deposit provide a valuable constraint on hydrodynamic parameters of tsunamis, including flow speed, flow depth and inundation distance, etc. (Li L et al., 2012, 2014; Sugawara and Goto, 2012). Inversion models and forward modelling could help in disclosing the tsunami impact and tsunamigenic mechanism (Dominey-Howes et al., 2006; Spiske et al., 2010; Srisutam and Wagner, 2010; Jaffe et al., 2011; Li L et al., 2014).

Finding paleo-tsunami deposits is very challenging in the SCS region. The challenge lies in two main issues: (1) The SCS region is located in the northwest Pacific region which is one of the regions most frequently hit by typhoons (Yang J et al., 2019). Distinguishing tsunami deposits from storm deposits thus become the main obstacle (Yang et al., 2021). (2) Many coastal areas in the SCS are densely populated and highly economically developed. Intense human activities including constructing infrastructures, land reclamation and nearshore aquaculture may have removed any possible tsunami deposits in coastal lowlands. So far, a few geologic and geomorphological studies have identified possible tsunami deposits in the SCS. These deposits are all located in offshore islands which are less disturbed by human activity (Yang et al., 2021). The reported locations include Dongdao Island (one of the Xisha Islands) (Sun et al., 2013), Nan'ao island (Yang W et al., 2019), Badoc island in the offshore Luzon island, Philippines (Ramos et al., 2017) and Penghu island (Lu et al., 2019). For the review of geological tsunami records in the SCS, please refer to Yang et al. (2021). One remarkable note is that the date of all these reported events is all around 1000 years ago. Whether these independent geo-

logical records were indeed produced by one tsunami event deserves more investigation. If the answer is positive, the spatial distribution of the geological evidence would imply the need for the earthquake to rupture a sufficiently large portion of the Manila Trench (Qiu et al., 2019; Yang et al., 2021). Tsunami deposits could be well-preserved in regions with favorable conditions, allowing the reconstruction of tsunami history during the Holocene (Rubin et al., 2017; Nakanishi et al., 2020). No geological evidence containing such long tsunami records has been discovered so far in the SCS. Researchers with diverse expertise in sedimentology, geochemistry, geophysics and fluid dynamics simulation are expected to continue unearthing the tsunami deposits in the inland region and deep sea, Such effort could ensure more scientific basis for the tsunami hazard assessment in the SCS.

6. Conclusions and future perspectives

This paper reviews the progress of tsunami hazard assessment for the megathrust earthquakes along the Manila Trench, nearshore earthquakes along the LFZ and submarine landslides. Through detailed analysis of representative earthquakes and submarine landslides scenarios, we summarize the main conclusions as follows:

(1) Earthquakes from the MSZ are the most probable sources for triggering ocean-wide tsunamis in the SCS. Due to the combined effects of tsunami directivity and the bathymetry, the coastal regions of south China (e.g., Guangdong, Fujian, Hainan and Guangxi), Taiwan island and islands inside the SCS would experience various degrees of damages. The coastal region of Guangdong province is among one of the worst-hit areas. The wave focusing effect caused by the local bathymetric hump right in front of the bay leads to a higher tsunami risk to the Greater Bay Area. Basin-wide resonance is expected due to the semi-enclosed nature of the SCS, resulting trapped tsunami energy and long-lasting oscillation in the basin. The existing tsunami hazard assessments suffer great uncertainties due to our limited knowledge of the seismogenic behaviours, geological structures, coupling ratio of the Manila Trench. Future research requires multiple disciplinary approaches including seafloor geodetic observation, 2D/3D seismic surveys, ocean drilling to investigate the fault geometries, kinematics, depth-dependent rock properties, and earthquake nucleation characteristics.

(2) The earthquakes initiated in the LFZ occur at a shallow water region which usually only trigger very localized tsunamis. Due to the unique seismogenic condition, when the initiated tsunami waves propagate from the shallow continental shelf region to the deep water in the SCS basin, the waves would be largely reflected back by the edge of continental slopes along the continental margin, and trapped in the continental shelf. The trapped tsunami waves would cause oscillation sustaining for a very long time period. The drastic rise and fall of sea water would induce strong wave currents along the southern coast of China, causing damages to infrastructures, harbors, and marinelands etc. Although geophysical surveys have been conducted to investigate the active faults in the northern SCS previously, the exact traces of these active faults, high-resolution geometrical structures and seismogenic characteristics remain poorly understood. Consequently, it is highly necessary to conduct comprehensive marine geophysical surveys of the active faults in the northern SCS including the LFZ, to gain knowledge on the 3D geological structure, the present activity and seismogenic behaviors of the major active faults. Such geophysical data ensures a more informed assessment of earthquake and tsunami hazard along the southern coast of China, and provide more solid scientific basis for the disaster prevention and mitigation planning.

(3) Numerous submarine landslides with various scales are extensively distributed in the continental slopes with different geological settings in the SCS. The unpredictable nature of submarine landslides challenges the current tsunami warning system. Large-scale submarine landslides could cause severe damage to submarine cables, ocean platforms and engineering in the deep sea and threaten coastal regions near the source. Tsunami hazard assessment for submarine landslides is still in the beginning stage in the SCS. To further construct the spatial and temporal distribution of landslides and establish a landslide database, more seafloor surveys including multi-beam seafloor surveys, 3D seismic surveys, and sediment coring and in-situ measurements are required. Integrated approaches of the seafloor surveys, physical experiments and numerical modelling techniques help better understand the triggering mechanism, instability and occurrence interval of submarine landslides. The formation mechanism, kinematic behaviour and disaster effect of identified landslides are to be investigated in the SCS.

The key challenge of assessing tsunami hazard in the SCS is our limited knowledge of the tsunami sources: the seismogenic characteristics of active faults and triggering mechanism of submarine landslides. Other aspects including the hydrodynamic features of tsunami wave propagation in the deep sea and nearshore (Ren et al., 2015; Liu et al., 2015; Wang et al., 2016), sediment transportation and deposition (Yang et al., 2021), and damaging effect on the coastal structures during the inundation process (Shen and Liu, 2018) all require more in-depth investigations. Compared with the inland geo-hazards of the same types, submarine earthquakes and landslides are more frequent, often with larger magnitudes. While restricted by the technological level of marine surveys and the high cost, we have very limited knowledge of their occurrences, generation mechanism and spatial distributions. Although tsunami hazard is infrequent

in the SCS, but the coastal region is highly economically developed and densely populated nowadays. It's very likely that a small tsunami event could cause a big disaster. The development of the petroleum, gas resource and marine fishery in the deep-sea area put forward the pressing needs of an improved understanding of marine geohazards. Investigating submarine earthquakes, landslides, and their associated tsunamis, therefore, is of great significance for disaster prevention and mitigation. Improving the capability of emergency response is also significant in terms of meeting the country's critical needs and ensuring the safety of people's lives and property.

Acknowledgements *This work was supported by the Guangdong Province Introduced Innovative R&D Team of Geological Processes and Natural Disasters around the South China Sea (Grant No. 2016ZT06N331), the Innovation Group Project of Southern Marine Science and Engineering Guangdong Laboratory (Zhuhai) (Grant No. 311021002), the Key Research and Development Program of Hainan Province (Grant No. ZDYF2020209), the National Natural Science Foundation of China (Grant Nos. 41976197, 42076059, 41774049, 41772209) and the Fundamental Research Funds for the Central Universities, Sun Yat-sen University (Grant No. 2021qntd23).*

References

Ammon C J, Kanamori H, Lay T. 2008. A great earthquake doublet and seismic stress transfer cycle in the central Kuril islands. Nature, 451: 561–565

An C. 2021. Tsunamis and tsunami warning: Recent progress and future prospects. Sci China Earth Sci, 64: 191–204

Armada L. 2016. Crustal structure and deformation in the Manila subduction zone. Tectonophysics, 466: 229–240

Atwater B F, Musumi-Rokkaku S, Satake K, Tsuji Y, Ueda K, Yamaguchi D. 2005. The Orphan Tsunami of 1700: Japanese clues to a parent earthquake in North America. US Geological Survey Professional Paper, 1707: 3–123

Basili R, Brizuela B, Herrero A, Iqbal S, Lorito S, Maesano F E, Murphy S, Perfetti P, Romano F, Scala A, Selva J, Taroni M, Tiberti M M, Thio H K, Tonini R, Volpe M, Glimsdal S, Harbitz C B, Løvholt F, Baptista M A, Carrilho F, Matias L M, Omira R, Babeyko A, Hoechner A, Gürbüz M, Pekcan O, Yalçıner A, Canals M, Lastras G, Agalos A, Papadopoulos G, Triantafyllou I, Benchekroun S, Agrebi Jaouadi H, Ben Abdallah S, Bouallegue A, Hamdi H, Oueslati F, Amato A, Armigliato A, Behrens J, Davies G, Di Bucci D, Dolce M, Geist E, Gonzalez Vida J M, González M, Macías Sánchez J, Meletti C, Ozer Sozdinler C, Pagani M, Parsons T, Polet J, Power W, Sørensen M, Zaytsev A. 2021. The making of the NEAM tsunami hazard model 2018 (NEAMTHM18). Front Earth Sci, 8: 1

Bautista M L P, Bartolome C,Bautista,Salcedo J C, Narag I. 2012. Philippine Tsunamis and Seiches. Philippine Institute of Volcanology and Seismology

Behrens J, Løvholt F, Jalayer F, Lorito S, Salgado-Gálvez M A, Sørensen M, Abadie S, Aguirre-Ayerbe I, Aniel-Quiroga I, Babeyko A, Baiguera M, Basili R, Belliazzi S, Grezio A, Johnson K, Murphy S, Paris R, Rafliana I, De Risi R, Rossetto T, Selva J, Taroni M, Del Zoppo M, Armigliato A, Bureš V, Cech P, Cecioni C, Christodoulides P, Davies G, Dias F, Bayraktar H B, González M, Gritsevich M, Guillas S, Harbitz C B, Kânoğlu U, Macías J, Papadopoulos G A, Polet J, Romano F, Salamon A, Scala A, Stepinac M, Tappin D R, Thio H K, Tonini R, Triantafyllou I, Ulrich T, Varini E, Volpe M, Vyhmeister E. 2021. Probabilistic tsunami hazard and risk analysis: A review of research gaps. Front Earth Sci, 9: 1

Bilek S L, Lay T. 2018. Subduction zone megathrust earthquakes. Geosphere, 14: 1468–1500

Bletery Q, Thomas A M, Rempel A W, Karlstrom L, Sladen A, De Barros L. 2016. Mega-earthquakes rupture flat megathrusts. Science, 354: 1027–1031

Cao J, Sun J, Xu H, Xia S. 2014. Seismognical features of the Littoral Fault Zone in the Pearl River Estuary(in Chinese). ChinJ Geophys, 57: 498–508

Cao J, Xia S, Sun J, Zhao F, Wan K, Xu H. 2018. Offshore fault geometrics in the Pearl River Estuary, Southeastern China: Evidence from seismic reflection data. J Ocean Univ China, 17: 799–810

Chamot-Rooke N, Le Pichon X. 1999. GPS determined eastward Sundaland motion with respect to Eurasia confirmed by earthquakes slip vectors at Sunda and Philippine trenches. Earth Planet Sci Lett, 173: 439–455

Chen C, Wu S, Zhao C. 2014. Incoming plate variation along the northern Manila Trench (in Chinese). Chin J Geophys, 57: 4063–4073

Chen D, Wang X, Völker D, Wu S, Wang L, Li W, Li Q, Zhu Z, Li C, Qin Z, Sun Q. 2016. Three dimensional seismic studies of deep-water hazard-related features on the northern slope of South China Sea. Mar Pet Geol, 77: 1125–1139

Chen E, Huang Y. 1984. Review of the 19 large earthquakes in southern China and the seismic belt in northern South China Sea (in Chinese). South China J Seismol, 4: 14–35

Chen E, Huang Y. 1989. The seismogenic structure and seismic hazard charateristic of the 1605 Qionghai earthquake(in Chinese). Acta Seismol Sin, 3: 319–331

Cheng G Y. 1830. Taiwan Interview Catalogue (in Chinese)

Chen H, He X, Yang H, Zhang J. 2021. Fault-plane determination of the 4 January 2020 offshore Pearl River Delta earthquake and its implication for seismic hazard assessment. Seismol Res Lett, 92: 1913–1925

Chen Y, Chen Q, Zhang W. 2007. Tsunami disaster in China (in Chinese). J Nat Disast, 16: 1–6

Cisternas M, Atwater B F, Torrejón F, Sawai Y, Machuca G, Lagos M, Eipert A, Youlton C, Salgado I, Kamataki T, Shishikura M, Rajendran C P, Malik J K, Rizal Y, Husni M. 2005. Predecessors of the giant 1960 Chile earthquake. Nature, 437: 404–407

Davies G, Griffin J. 2018. The 2018 Australian probabilistic tsunami hazard assessment: Hazard from earthquake generated tsunamis. Pure Appl Geophys,177: 1–28

Davies G, Griffin J. 2020. Sensitivity of probabilistic tsunami hazard assessment to far-field earthquake slip complexity and rigidity depth-dependence: Case study of Australia. Pure Appl Geophys, 177: 1521–1548

Dogan G G, Yalciner A C, Yuksel Y, Ulutaş E, Polat O, Güler I ı, Şahin C, Tarih A, Kânoğlu U. 2021. The 30 October 2020 Aegean Sea tsunami: Post-event field survey along Turkish Coast. Pure Appl Geophys, 178: 785–812

Dominey-Howes D T M, Humphreys G S, Hesse P P. 2006. Tsunami and palaeotsunami depositional signatures and their potential value in understanding the late-Holocene tsunami record. Holocene, 16: 1095–1107

Enet F, Grilli S T. 2007. Experimental study of tsunami generation by three-dimensional rigid underwater landslides. J Water Port Coast Ocean Eng, 133: 442–454

Fan W, Bassett D, Jiang J, Shearer P M, Ji C. 2017. Rupture evolution of the 2006 Java tsunami earthquake and the possible role of splay faults. Tectonophysics, 721: 143–150

Fine I V, Rabinovich A B, Bornhold B D, Thomson R E, Kulikov E A. 2005. The Grand Banks landslide-generated tsunami of November 18, 1929: Preliminary analysis and numerical modeling. Mar Geol, 215: 45–57

Fine I V, Rabinovich A B, Thomson R E, Kulikov E A. 2003. Numerical modeling of tsunami generation by submarine and subaerial landslides. Submar Landsl Tsunamis, 21: 69–88

Fukutani Y, Suppasri A, Imamura F. 2014. Stochastic analysis and uncertainty assessment of tsunami wave height using a random source parameter model that targets a Tohoku-type earthquake fault. Stoch

Environ Res Risk Assess, 29: 1763–1779
Gagnon K, Chadwell C D, Norabuena E. 2005. Measuring the onset of locking in the Peru-Chile trench with GPS and acoustic measurements. Nature, 434: 205–208
Gao J, Wu S, Yao Y, Chen C, Song T, Wang J, Sun J, Zhang H, Ma B, Xie Y. 2018. Tectonic deformation and fine structure of the frontal accretionary wedge, northern Manila subduction zone (in Chinese). Chin J Geophys, 61: 2845–2858
Gee M J R, Uy H S, Warren J, Morley C K, Lambiase J J. 2007. The Brunei slide: A giant submarine landslide on the North West Borneo Margin revealed by 3D seismic data. Mar Geol, 246: 9–23
Geersen J. 2019. Sediment-starved trenches and rough subducting plates are conducive to tsunami earthquakes. Tectonophysics, 762: 28–44
Geist E L, Lynett P J, Chaytor J D. 2009. Hydrodynamic modeling of tsunamis from the Currituck landslide. Mar Geol, 264: 41–52
Geist E, Lynett P. 2014. Source processes for the probabilistic assessment of tsunami hazards. Oceanography, 27: 86–93
Geist E L, Parsons T E. 2010. Estimating the empirical probability of submarine landslide occurrence. Submar Mass Movement Their Consequences, 28: 377–386
Geist E L. 2002. Complex earthquake rupture and local tsunamis. J Geophys Res, 107: 2086
Gibbons S J, Lorito S, Macías J, Løvholt F, Selva J, Volpe M, Sánchez-Linares C, Babeyko A, Brizuela B, Cirella A, Castro M J, de la Asunción M, Lanucara P, Glimsdal S, Lorenzino M C, Nazaria M, Pizzimenti L, Romano F, Scala A, Tonini R, Manuel González Vida J, Vöge M. 2020. Probabilistic tsunami hazard analysis: High performance computing for massive scale inundation simulations. Front Earth Sci, 8: 1
Goda K, Song J. 2016. Uncertainty modeling and visualization for tsunami hazard and risk mapping: A case study for the 2011 Tohoku earthquake. Stoch Environ Res Risk Assess, 30: 2271–2285
Goda K, Yasuda T, Mori N, Mai P M. 2015. Variability of tsunami inundation footprints considering stochastic scenarios based on a single rupture model: Application to the 2011 Tohoku earthquake. J Geophys Res-Oceans, 120: 4552–4575
Goff J, Chagué-Goff C, Dominey-Howes D, McAdoo B, Cronin S, Bonté-Grapetin M, Nichol S, Horrocks M, Cisternas M, Lamarche G, Pelletier B, Jaffe B, Dudley W. 2011. Palaeotsunamis in the Pacific Islands. Earth-Sci Rev, 107: 141–146
González F I, Geist E L, Jaffe B, Kânoğlu U, Mofjeld H, Synolakis C E, Titov V V, Arcas D, Bellomo D, Carlton D, Horning T, Johnson J, Newman J, Parsons T, Peters R, Peterson C, Priest G, Venturato A, Weber J, Wong F, Yalciner A. 2009. Probabilistic tsunami hazard assessment at Seaside, Oregon, for near- and far-field seismic sources. J Geophys Res, 114: C11023
González M, Álvarez-Gómez J A, Aniel-Quiroga Í, Otero L, Olabarrieta M, Omira R, Luceño A, Jelinek R, Krausmann E, Birkman J, Baptista M A, Miranda M, Aguirre-Ayerbe I. 2021. Probabilistic tsunami hazard assessment in meso and macro tidal areas. Application to the Cádiz Bay, Spain. Front Earth Sci, 9: 328
Goto K, Sugawara D, Ikema S, Miyagi T. 2012. Sedimentary processes associated with sand and boulder deposits formed by the 2011 Tohoku-oki tsunami at Sabusawa Island, Japan. Sediment Geol, 282: 188–198
Grezio A, Babeyko A, Baptista M A, Behrens J, Costa A, Davies G, Geist E L, Glimsdal S, González F I, Griffin J, Harbitz C B, LeVeque R J, Lorito S, Løvholt F, Omira R, Mueller C, Paris R, Parsons T, Polet J, Power W, Selva J, Sørensen M B, Thio H K. 2017. Probabilistic tsunami hazard analysis: Multiple sources and global applications. Rev Geophys, 55: 1158–1198
Grezio A, Cinti F R, Costa A, Faenza L, Perfetti P, Pierdominici S, Pondrelli S, Sandri L, Tierz P, Tonini R, Selva J. 2020. Multisource Bayesian probabilistic tsunami hazard analysis for the Gulf of Naples (Italy). J Geophys Res-Oceans, 125: e2019JC015373
Grezio A, Sandri L, Marzocchi W, Argnani A, Gasparini P, Selva J. 2012. Probabilistic tsunami hazard assessment for Messina Strait Area (Sicily, Italy). Nat Hazards, 64: 329–358
Grilli S T, Taylor O D S, Baxter C D P, Maretzki S. 2009. A probabilistic approach for determining submarine landslide tsunami hazard along the upper east coast of the United States. Mar Geol, 264: 74–97
Grilli S T, Shelby M, Kimmoun O, Dupont G, Nicolsky D, Ma G, Kirby J T, Shi F. 2017. Modeling coastal tsunami hazard from submarine mass failures: Effect of slide rheology, experimental validation, and case studies off the US East Coast. Nat Hazards, 86: 353–391
Hananto N D, Leclerc F, Li L, Etchebes M, Carton H, Tapponnier P, Qin Y, Avianto P, Singh S C, Wei S. 2020. Tsunami earthquakes: Vertical pop-up expulsion at the forefront of subduction megathrust. Earth Planet Sci Lett, 538: 116197
Harbitz C B, Løvholt F, Bungum H. 2014. Submarine landslide tsunamis: How extreme and how likely? Nat Hazards, 72: 1341–1374
He Y, Zhong G, Wang L, Kuang Z. 2014. Characteristics and occurrence of submarine canyon-associated landslides in the middle of the northern continental slope, South China Sea. Mar Pet Geol, 57: 546–560
Heidarzadeh M, Satake K. 2014. Excitation of basin-wide modes of the Pacific Ocean following the March 2011 Tohoku tsunami. Pure Appl Geophys, 171: 3405–3419
Hill E M, Borrero J C, Huang Z, Qiu Q, Banerjee P, Natawidjaja D H, Elosegui P, Fritz H M, Suwargadi B W, Pranantyo I R, Li L L, Macpherson K A, Skanavis V, Synolakis C E, Sieh K. 2012. The 2010 M_w7.8 Mentawai earthquake: Very shallow source of a rare tsunami earthquake determined from tsunami field survey and near-field GPS data. J Geophys Res, 117: B06402
Hsu S K, Kuo J, Yeh Y C, Tsai C H, Doo W, Ku C Y, Sibuet J C. 2008. Turbidity currents, submarine landslides and the 2006 Pingtung Earthquake off SW Taiwan. Terr Atmos Ocean Sci, 19: 767–772
Hsu Y J, Yu S B, Song T R A, Bacolcol T. 2012. Plate coupling along the Manila subduction zone between Taiwan and northern Luzon. J Asian Earth Sci, 51: 98–108
Hsu Y J, Yu S B, Loveless J P, Bacolcol T, Solidum R, Luis Jr A, Pelicano A, Woessner J. 2016. Interseismic deformation and moment deficit along the Manila subduction zone and the Philippine Fault system. J Geophys Res-Solid Earth, 121: 7639–7665
Huang X, Betzler C, Wu S, Bernhardt A, Eagles G, Han X, Hovland M. 2020. First documentation of seismic stratigraphy and depositional signatures of Zhongsha atoll (Macclesfield Bank), South China Sea. Mar Pet Geol, 117: 104349
Huang Z, Wu T R, Tan S K, Megawati K, Shaw F, Liu X, Pan T C. 2009. Tsunami hazard from the subduction Megathrust of the South China Sea: Part II. Hydrodynamic modeling and possible impact on Singapore. J Asian Earth Sci, 36: 93–97
Hubbard J, Barbot S, Hill E M, Tapponnier P. 2015. Coseismic slip on shallow décollement megathrusts: Implications for seismic and tsunami hazard. Earth-Sci Rev, 141: 45–55
Jaffe B, Buckley M, Richmond B, Strotz L, Etienne S, Clark K, Watt S, Gelfenbaum G, Goff J. 2011. Flow speed estimated by inverse modeling of sandy sediment deposited by the 29 September 2009 tsunami near Satitoa, east Upolu, Samoa. Earth-Sci Rev, 107: 23–37
Jankaew K, Atwater B F, Sawai Y, Choowong M, Charoentitirat T, Martin M E, Prendergast A. 2008. Medieval forewarning of the 2004 Indian Ocean tsunami in Thailand. Nature, 455: 1228–1231
Kelsey H M, Nelson A R, Hemphill-Haley E, Witter R C. 2005. Tsunami history of an Oregon coastal lake reveals a 4600 yr record of great earthquakes on the Cascadia subduction zone. GSA Bull, 117: 1009–1032
Kim J, Løvholt F, Issler D, Forsberg C F. 2019. Landslide material control on tsunami genesis—The Storegga Slide and Tsunami (8,100 years BP). J Geophys Res-Oceans, 124: 3607–3627
Lane E M, Mountjoy J J, Power W L, Mueller C. 2017. Probabilistic Hazard of Tsunamis Generated by Submarine Landslides in the Cook Strait Canyon (New Zealand). In: Geist E L, Fritz H M, Rabinovich A B, Tanioka Y, eds. Global Tsunami Science: Past and Future, Volume I. Cham: Birkhäuser. 3757–3774
Lau A Y A, Switzer A D, Dominey-Howes D, Aitchison J C, Zong Y. 2010. Written records of historical tsunamis in the northeastern South China

Sea-challenges associated with developing a new integrated database. Nat Hazards Earth Syst Sci, 10: 1793–1806
Lay T. 2018. A review of the rupture characteristics of the 2011 Tohoku-oki M_w9.1 earthquake. Tectonophysics, 733: 4–36
Leonard L J, Rogers G C, Mazzotti S. 2014. Tsunami hazard assessment of Canada. Nat Hazards, 70: 237–274
Leslie S C, Mann P. 2016. Giant submarine landslides on the Colombian margin and tsunami risk in the Caribbean Sea. Earth Planet Sci Lett, 449: 382–394
Li H, Yuan Y, Xu Z, Wang Z, Wang J, Wang P, Gao Y, Hou J, Shan D. 2017. The dependency of probabilistic tsunami hazard assessment on magnitude limits of seismic sources in the South China Sea and adjoining basins. Pure Appl Geophys, 174: 2351–2370
Li L, Qiu Q, Huang Z. 2012. Numerical modeling of the morphological change in Lhok Nga, west Banda Aceh, during the 2004 Indian Ocean tsunami: Understanding tsunami deposits using a forward modeling method. Nat Hazards, 64: 1549–1574
Li L, Huang Z, Qiu Q. 2014. Numerical simulation of erosion and deposition at the Thailand Khao Lak coast during the 2004 Indian Ocean tsunami. Nat Hazards, 74: 2251–2277
Li L, Li F, Qiu Q, Li Z, Zhang D, Hui G. 2022. Tsunami simulation of the 1918 Nan'ao earthquake and its implication (in Chinese). Acta Scient Natural Univ Sunyat, 61: 27–38
Li L, Shi F, Ma G, Qiu Q. 2019. Tsunamigenic potential of the Baiyun Slide complex in the South China Sea. J Geophys Res-Solid Earth, 124: 7680–7698
Li L, Switzer A D, Chan C H, Wang Y, Weiss R, Qiu Q. 2016. How heterogeneous coseismic slip affects regional probabilistic tsunami hazard assessment: A case study in the South China Sea. J Geophys Res-Solid Earth, 121: 6250–6272
Li L, Switzer A D, Wang Y, Chan C H, Qiu Q, Weiss R. 2018. A modest 0.5-m rise in sea level will double the tsunami hazard in Macau. Sci Adv, 4: eaat1180
Li L, Switzer A D, Wang Y, Weiss R, Qiu Q, Chan C H, Tapponnier P. 2015. What caused the mysterious eighteenth century tsunami that struck the southwest Taiwan coast? Geophys Res Lett, 42: 8498–8506
Li W, Alves T M, Wu S, Völker D, Zhao F, Mi L, Kopf A. 2015. Recurrent slope failure and submarine channel incision as key factors controlling reservoir potential in the South China Sea (Qiongdongnan Basin, South Hainan Island). Mar Pet Geol, 64: 17–30
Li W, Wu S, Völker D, Zhao F, Mi L, Kopf A. 2014a. Morphology, seismic characterization and sediment dynamics of the Baiyun Slide Complex on the northern South China Sea margin. J Geol Soc, 171: 865–877
Li W, Wu S, Wang X, Zhao F, Wang D, Mi L, Li Q. 2014b. Baiyun slide and its relation to fluid migration in the northern slope of Southern China Sea. In: Krastel S, Behrmann J H, Völker D, Stipp M, Berndt C, Urgeles R, Chaytor J, Huhn K, Strasser M, Harbitz C B, eds. Submarine Mass Movements and Their Consequences: 6th International Symposium. Springer International Publishing. 105–115
Li X, Wang D, Wu S, Wang W, Liu G. 2017. Canyon indentification and seafloor geomophology analysis in Sansha (in Chinese). Mar Geol Quat Geol, 37: 28–36
Lin A T, Yao B, Hsu S K, Liu C S, Huang C Y. 2009. Tectonic features of the incipient arc-continent collision zone of Taiwan: Implications for seismicity. Tectonophysics, 479: 28–42
Lin J, Xu M, Zhou Z, Wang Y. 2017. Ocean drilling investigation of the global subduction processes (in Chinese). Adv Earth Sci, 12: 1253–1266
Liu H, Zhao X, Wang B, Ren Z. 2015. Numercial modeling of tsunami wave and tsunami warning approach in the South China Sea (in Chinese). Chin Quart Mechan, 36: 351–369
Liu P L F, Higuera P, Husrin S, Prasetya G S, Prihantono J, Diastomo H, Pryambodo D G, Susmoro H. 2020. Coastal landslides in Palu Bay during 2018 Sulawesi earthquake and tsunami. Landslides, 17: 2085–2098
Liu P L F, Wang X, Salisbury A J. 2009. Tsunami hazard and early warning system in South China Sea. J Asian Earth Sci, 36: 2–12
Liu P L F, Woo S B, Cho Y S. 1998. Computer programs for tsunami propagation and inundation. Technical Report. Cornell University
Liu Y, Santos A, Wang S M, Shi Y, Liu H, Yuen D A. 2007. Tsunami hazards along Chinese coast from potential earthquakes in South China Sea. Phys Earth Planet Inter, 163: 233–244
Liu Y. 1981. Fault Structure Analysis Along Southern Coast of China (in Chinese). Beijing: Seismological Press
Liu Y. 1985. Active faults along southern coast of China (in Chinese). Mar Geol Quat Geol, 3: 13–23
Løvholt F, Bondevik S, Laberg J S, Kim J, Boylan N. 2017. Some giant submarine landslides do not produce large tsunamis. Geophys Res Lett, 44: 8463–8472
Løvholt F, Glimsdal S, Harbitz C B. 2020. On the landslide tsunami uncertainty and hazard. Landslides, 17: 2301–2315
Løvholt F, Pedersen G, Harbitz C B, Glimsdal S, Kim J. 2015. On the characteristics of landslide tsunamis. Phil Trans R Soc A, 373: 20140376
Løvholt F, Schulten I, Mosher D, Harbitz C, Krastel S. 2019. Modelling the 1929 Grand Banks slump and landslide tsunami. Geol Soc Lond Spec Publ, 477: 315–331
Lu C H, Yen J Y, Chyi S J, Yu N T, Chen J H. 2019. Geological records of South China Sea tsunamis on Penghu Islands, Taiwan. J Asian Earth Sci, 177: 263–274
Ma G, Shi F, Kirby J T. 2012. Shock-capturing non-hydrostatic model for fully dispersive surface wave processes. Ocean Model, 43-44: 22–35
Mallet R. 1854. Third report of the facts of earthquake phenomena. Catalogue of recorded earthquakes from 1606B.C. to A.D.1850 (1755–1784). Reports of the British Association Meetings, 22: 1–176 (1852)
Maselli V, Oppo D, Moore A L, Gusman A R, Mtelela C, Iacopini D, Taviani M, Mjema E, Mulaya E, Che M, Tomioka A L, Mshiu E, Ortiz J D. 2020. A 1000-yr-old tsunami in the Indian Ocean points to greater risk for East Africa. Geology, 48: 808–813
McCaffrey R. 2008. Global frequency of magnitude 9 earthquakes. Geology, 36: 263–266
McSaveney M J, Goff J R, Darby D J, Goldsmith P, Barnett A, Elliott S, Nongkas M. 2000. The 17 July 1998 tsunami, Papua New Guinea: Evidence and initial interpretation. Mar Geol, 170: 81–92
Megawati K, Shaw F, Sieh K, Huang Z, Wu T R, Lin Y, Tan S K, Pan T C. 2009. Tsunami hazard from the subduction megathrust of the South China Sea: Part I. Source characterization and the resulting tsunami. J Asian Earth Sci, 36: 13–20
Meltzner A J, Sieh K, Chiang H W, Shen C C, Suwargadi B W, Natawidjaja D H, Philibosian B, Briggs R W. 2012. Persistent termini of 2004- and 2005-like ruptures of the Sunda megathrust. J Geophys Res, 117: B04405
Meltzner A J, Sieh K, Chiang H W, Shen C C, Suwargadi B W, Natawidjaja D H, Philibosian B E, Briggs R W, Galetzka J. 2010. Coral evidence for earthquake recurrence and an A.D. 1390–1455 cluster at the south end of the 2004 Aceh-Andaman rupture. J Geophys Res-Solid Earth, 115: B10402
Moore G F, Bangs N L, Taira A, Kuramoto S, Pangborn E, Tobin H J. 2007. Three-dimensional splay fault geometry and implications for tsunami generation. Science, 318: 1128–1131
Mori N, Goda K, Cox D. 2018. Recent process in Probabilistic Tsunami Hazard Analysis (PTHA) for mega thrust subduction earthquakes. Adv Nat Technol Hazards Res, 47: 469–485
Mueller C, Mountjoy J, Power W, Lane E, Wang X. 2016. Towards a spatial probabilistic submarine landslide hazard model for submarine canyons. In: Lamarche G, Mountjoy J, Bull S, Hubble T, Krastel S, Lane E, Micallef A, Moscardelli L, Mueller C, Pecher I, Woelz S, eds. Submarine Mass Movements and their Consequences: 7th International Symposium. Springer International Publishing. 589–597
Mueller C, Power W, Fraser S, Wang X. 2015. Effects of rupture complexity on local tsunami inundation: Implications for probabilistic tsunami hazard assessment by example. J Geophys Res-Solid Earth, 120: 488–502
Murphy S, Scala A, Herrero A, Lorito S, Festa G, Trasatti E, Tonini R,

Romano F, Molinari I, Nielsen S. 2016. Shallow slip amplification and enhanced tsunami hazard unravelled by dynamic simulations of mega-thrust earthquakes. Sci Rep, 6: 35007
Nakanishi R, Okamura S, Yokoyama Y, Miyairi Y, Sagayama T, Ashi J. 2020. Holocene tsunami, storm, and relative sea level records obtained from the southern Hidaka coast, Hokkaido, Japan. Quat Sci Rev, 250: 106678
Nanayama F, Furukawa R, Shigeno K, Makino A, Soeda Y, Igarashi Y. 2007. Nine unusually large tsunami deposits from the past 4000 years at Kiritappu marsh along the southern Kuril Trench. Sediment Geol, 200: 275–294
Nanayama F, Satake K, Furukawa R, Shimokawa K, Atwater B F, Shigeno K, Yamaki S. 2003. Unusually large earthquakes inferred from tsunami deposits along the Kuril trench. Nature, 424: 660–663
Nanto D, Cooper W, Donnelly M, Johnson R. 2011. Japan's 2011 earthquake and tsunami: Economic effects and implications for the United States. DIANE Publishing
Nguyen P H, Bui Q C, Vu P H, Pham T T. 2014. Scenario-based tsunami hazard assessment for the coast of Vietnam from the Manila Trench source. Phys Earth Planet Inter, 236: 95–108
Obana K, Kodaira S. 2009. Low-frequency tremors associated with reverse faults in a shallow accretionary prism. Earth Planet Sci Lett, 287: 168–174
Okal E A, Synolakis C E, Kalligeris N. 2011. Tsunami simulations for regional sources in the South China and adjoining seas. Pure Appl Geophys, 168: 1153–1173
Pampell-Manis A, Horrillo J, Shigihara Y, Parambath L. 2016. Probabilistic assessment of landslide tsunami hazard for the northern Gulf of Mexico. J Geophys Res-Oceans, 121: 1009–1027
Paris R, Fournier J, Poizot E, Etienne S, Morin J, Lavigne F, Wassmer P. 2010. Boulder and fine sediment transport and deposition by the 2004 tsunami in Lhok Nga (western Banda Aceh, Sumatra, Indonesia): A coupled offshore-onshore model. Mar Geol, 268: 43–54
Paris R, Switzer A D, Belousova M, Belousov A, Ontowirjo B, Whelley P L, Ulvrova M. 2014. Volcanic tsunami: A review of source mechanisms, past events and hazards in Southeast Asia (Indonesia, Philippines, Papua New Guinea). Nat Hazards, 70: 447–470
Park H, Cox D T. 2016. Probabilistic assessment of near-field tsunami hazards: Inundation depth, velocity, momentum flux, arrival time, and duration applied to Seaside, Oregon. Coast Eng, 117: 79–96
Peng C, Li Y, Wu M. 2017. Analysis of seismogenic structure mechanism of the Nan'ao earthquake in 1918 (in Chinese). South China J Seismol, 37: 1–14
Perrey A. 1862. Documents sur les tremblements de terre et les phenomenos volcaniques au Japon (in French)
Philibosian B, Meltzner A J. 2020. Segmentation and supercycles: A catalog of earthquake rupture patterns from the Sumatran Sunda Megathrust and other well-studied faults worldwide. Quat Sci Rev, 241: 106390
Pope E L, Talling P J, Urlaub M, Hunt J E, Clare M A, Challenor P. 2015. Are large submarine landslides temporally random or do uncertainties in available age constraints make it impossible to tell? Mar Geol, 369: 19–33
Power W, Horspool N, Wang X, Mueller C. 2015. Probabilistic mapping of tsunami hazard and risk for gisborne city and wainui beach. GNS Sci Consultancy Report, 219: 79
Qiu Q, Li L, Hsu Y J, Wang Y, Chan C H, Switzer A D. 2019. Revised earthquake sources along Manila trench for tsunami hazard assessment in the South China Sea. Nat Hazards Earth Syst Sci, 19: 1565–1583
Qiu Z, Han X, Wang Y, Tao C. 2009. Research progress in tsunami warning and Quaternary paleo-tsunami sedimentary records (in Chinese). J Mar Sci,27: 67–73
Ramos N T, Maxwell K V, Tsutsumi H, Chou Y C, Duan F, Shen C C, Satake K. 2017. Occurrence of 1 ka-old corals on an uplifted reef terrace in west Luzon, Philippines: Implications for a prehistoric extreme wave event in the South China Sea region. Geosci Lett, 4: 12
Ren J, Sun M, Han B. 2021. A giant submarine landslide and its triggering mechanisms on the Nansha trough margin, south China Sea (in Chinese). Earth Sci, 46: 1058–1071
Ren L, Huo Z, Hong M. 2014. Principle and method of the seismic tsunami hazard analysis coupling uncertainty effect of potential source parameters (in Chinese). Mar Forec, 31: 7–13
Ren Y, Wen R, Song Y. 2014. Recent progress of tsunami hazard mitigation in China. Episodes, 37: 277–283
Ren Y, Wen R, Zhang P, Yang Z, Pan R, Li X. 2016. Implications of local sources to probabilistic tsunami hazard analysis in South Chinese coastal area. J Earthquake Tsunami, 11: 1740001
Ren Y, Zhao M, Zhang J, Lv Z, Pang X, Qiu X. 2020. Constraint on the shape of the Manila subduction slab from earthquake relocation using long-term ocean bottom seismometer data (in Chinese). Chin J Geophys, 63: 1927–1937
Ren Z Y, Zhao X, Liu H. 2015. Dispersion effects on tsunami propagation in south China sea. J Earthquake Tsunami, 9: 1540001
Ren Z, Zhao X, Liu H. 2019. Numerical study of the landslide tsunami in the South China Sea using Herschel-Bulkley rheological theory. Phys Fluids, 31: 056601
Ren Z, Zhao X, Liu H. 2018. Numerical study of submarine landslide tsunami based on rheological theory (in Chinese). Chin Quart Mechan, 39: 451–464
Richmond B, Szczuciński W, Chagué-Goff C, Goto K, Sugawara D, Witter R, Tappin D R, Jaffe B, Fujino S, Nishimura Y, Goff J. 2012. Erosion, deposition and landscape change on the Sendai coastal plain, Japan, resulting from the March 11, 2011 Tohoku-oki tsunami. Sediment Geol, 282: 27–39
Rubin C M, Horton B P, Sieh K, Pilarczyk J E, Daly P, Ismail N, Parnell A C. 2017. Highly variable recurrence of tsunamis in the 7,400 years before the 2004 Indian Ocean tsunami. Nature Communications 2017 8:1, 8: 1–12
Saito T, Inazu D, Tanaka S, Miyoshi T. 2013. Tsunami coda across the Pacific Ocean following the 2011 Tohoku-Oki earthquake. Bull Seismol Soc Am, 103: 1429–1443
Satake K, Atwater B F. 2007. Long-term perspectives on giant earthquakes and tsunamis at subduction zones. Annu Rev Earth Planet Sci, 35: 349–374
Satake K, Nanayama F, Yamaki S, Tanioka Y, Hirata K. 2005. Variability Among Tsunami Sources in the 17th-21st Centuries Along the Soutehrn Kuril Trench. In Kenji Satake (Ed.), Tsunamis (Vol. 23, pp. 157-170). Springer Netherlands
Satake K, Wang K, Atwater B F. 2003. Fault slip and seismic moment of the 1700 Cascadia earthquake inferred from Japanese tsunami descriptions. J Geophys Res, 108: 2535
Satake K, Shimazaki K. 1988. Free oscillation of the Japan Sea excited by earthquakes—I. Observation and wave-theoretical approach. Geophys J Int, 93: 451–456
Schambach L, Grilli S T, Kirby J T, Shi F. 2018. Landslide tsunami hazard along the upper US east coast: Effects of slide deformation, bottom friction, and frequency dispersion. Pure Appl Geophys, 176: 3059–3098
Schambach L, Grilli S T, Tappin D R. 2021. New high-resolution modeling of the 2018 Palu tsunami, based on supershear earthquake mechanisms and mapped coastal landslides, supports a dual source. Front Earth Sci, 627
Schellart W P, Rawlinson N. 2013. Global correlations between maximum magnitudes of subduction zone interface thrust earthquakes and physical parameters of subduction zones. Phys Earth Planet Inter, 225: 41–67
Sepúlveda I, Haase J S, Liu P L E, Grigoriu M, Winckler P. 2021. Non-stationary probabilistic tsunami hazard assessments incorporating climate-change-driven sea level rise. Earths Future, 9: e02007
Sepúlveda I, Liu P L E, Grigoriu M. 2019. Probabilistic tsunami hazard assessment in South China Sea with consideration of uncertain earthquake characteristics. J Geophys Res-Solid Earth, 124: 658–688
Shelley K, Segall P. 2000. A mechanical model for intraplate earthquakes: Application to the New Madrid seismic zone. Science, 289: 2329–2332
Shen J, Liu H. 2018. Relationship between wave face angle and force

investigation when tsunami interacts with vertical wall (in Chinese). CSTAM-2018-D036. Hangzhou, China
Shi F, Kirby J T, Harris J C, Geiman J D, Grilli S T. 2012. A high-order adaptive time-stepping TVD solver for Boussinesq modeling of breaking waves and coastal inundation. Ocean Model, 43-44: 36–51
Shi H, Si P, Dong P, Yu X. 2019. A two-phase SPH model for massive sediment motion in free surface flows. Adv Water Resources, 129: 80–98
Si P, Shi H, Yu X. 2018. A general numerical model for surface waves generated by granular material intruding into a water body. Coast Eng, 142: 42–51
Sieh K, Natawidjaja D H, Meltzner A J, Shen C C, Cheng H, Li K S, Suwargadi B W, Galetzka J, Philibosian B, Edwards R L. 2008. Earthquake supercycles inferred from sea-level changes recorded in the corals of west Sumatra. Science, 322: 1674–1678
Sørensen M B, Spada M, Babeyko A, Wiemer S, Grünthal G. 2012. Probabilistic tsunami hazard in the Mediterranean Sea. J Geophys Res-Solid Earth, 117: B01305
Spiske M, Weiss R, Bahlburg H, Roskosch J, Amijaya H. 2010. The TsuSedMod inversion model applied to the deposits of the 2004 Sumatra and 2006 Java tsunami and implications for estimating flow parameters of palaeo-tsunami. Sediment Geol, 224: 29–37
Srisutam C, Wagner J F. 2010. Reconstructing tsunami run-up from the characteristics of tsunami deposits on the Thai Andaman Coast. Coast Eng, 57: 493–499
Su C C, Tseng J Y, Hsu H H, Chiang C S, Yu H S, Lin S, Liu J T. 2012. Records of submarine natural hazards off SW Taiwan. Geol Soc Lond Spec Publ, 361: 41–60
Sugawara D, Goto K. 2012. Numerical modeling of the 2011 Tohoku-oki tsunami in the offshore and onshore of Sendai Plain, Japan. Sediment Geol, 282: 110–123
Sun J, Xu H, Zhan W, Cao J. 2012. Activity and triggering mechanism of seismic belt along the northern South China Sea continental margin (in Chinese). J Trop Oceanogr, 31: 40–47
Sun L, Zhou X, Huang W, Liu X, Yan H, Xie Z, Wu Z, Zhao S, Da Shao S, Yang W. 2013. Preliminary evidence for a 1000-year-old tsunami in the South China Sea. Sci Rep, 3: 1655
Sun Q, Alves T M, Lu X, Chen C, Xie X. 2018a. True volumes of slope failure estimated from a Quaternary mass-transport deposit in the Northern South China Sea. Geophys Res Lett, 45: 2642–2651
Sun Q, Cartwright J, Xie X, Lu X, Yuan S, Chen C. 2018b. Reconstruction of repeated Quaternary slope failures in the northern South China Sea. Mar Geol, 401: 17–35
Sun Q, Leslie S. 2020. Tsunamigenic potential of an incipient submarine slope failure in the northern South China Sea. Mar Pet Geol, 112: 104111
Sun Q, Xie X, Piper D J W, Wu J, Wu S. 2017. Three dimensional seismic anatomy of multi-stage mass transport deposits in the Pearl River Mouth Basin, northern South China Sea: Their ages and kinematics. Mar Geol, 393: 93–108
Sun Y, Huang B. 2014. A potential tsunami impact assessment of submarine landslide at Baiyun Depression in Northern South China Sea. GEOENVIRON DISASTERS, 1: 7
Synolakis C E, Bardet J P, Borrero J C, Davies H L, Okal E A, Silver E A, Sweet S, Tappin D R. 2002. The slump origin of the 1998 Papua New Guinea tsunami. Proc R Soc Lond A, 458: 763–789
Tan W K, Teh S Y, Koh H L. 2017. Tsunami run-up and inundation along the coast of Sabah and Sarawak, Malaysia due to a potential Brunei submarine mass failure. Environ Sci Pollut Res, 24: 15976–15994
Tappin D R, Watts P, McMurtry G M, Lafoy Y, Matsumoto T. 2001. The Sissano, Papua New Guinea tsunami of July 1998—Offshore evidence on the source mechanism. Mar Geol, 175: 1–23
Taylor F W, Briggs R W, Frohlich C, Brown A, Hornbach M, Papabatu A K, Meltzner A J, Billy D. 2008. Rupture across arc segment and plate boundaries in the 1 April 2007 Solomons earthquake. Nat Geosci, 1: 253–257
ten Brink U S, Barkan R, Andrews B D, Chaytor J D. 2009. Size distributions and failure initiation of submarine and subaerial landslides. Earth Planet Sci Lett, 287: 31–42
ten Brink U S, Chaytor J D, Geist E L, Brothers D S, Andrews B D. 2014. Assessment of tsunami hazard to the U.S. Atlantic margin. Mar Geol, 353: 31–54
ten Brink U S, Geist E L, Andrews B D. 2006. Size distribution of submarine landslides and its implication to tsunami hazard in Puerto Rico. Geophys Res Lett, 33: 2006GL026125
Terry J P, Winspear N, Goff J, Tan P H H. 2017. Past and potential tsunami sources in the South China Sea: A brief synthesis. Earth-Sci Rev, 167: 47–61
Thio H K, Somerville P, Ichinose G. 2007. Probabilistic analysis of strong ground motion and tsunami hazards in southeast Asia. J Earthquake Tsunami, 01: 119–137
Titov V, Rabinovich A B, Mofjeld H O, Thomson R E, Gonzalez F I. 2005. The global reach of the 26 December 2004 Sumatra tsunami. Science, 309: 2045–2048
Urgeles R, Camerlenghi A. 2013. Submarine landslides of the Mediterranean Sea: Trigger mechanisms, dynamics, and frequency-magnitude distribution. J Geophys Res-Earth Surf, 118: 2600–2618
Urlaub M, Talling P J, Masson D G. 2013. Timing and frequency of large submarine landslides: Implications for understanding triggers and future geohazard. Quat Sci Rev, 72: 63–82
Volpe M, Lorito S, Selva J, Tonini R, Romano F, Brizuela B. 2019. From regional to local SPTHA: Efficient computation of probabilistic tsunami inundation maps addressing near-field sources. Nat Hazards Earth Syst Sci, 19: 455–469
Vu T C, Nguyen D X. 2008. Tsunami risk along Vietnamese coast. J Water Resour Environ Eng, 23: 24–33
Wallace L M, Webb S C, Ito Y, Mochizuki K, Hino R, Henrys S, Schwartz S Y, Sheehan A F. 2016. Slow slip near the trench at the Hikurangi subduction zone, New Zealand. Science, 352: 701–704
Wang D, Wu S, Qin Z, Spence G, Lü F. 2013. Seismic characteristics of the Huaguang mass transport deposits in the Qiongdongnan Basin, South China Sea: Implications for regional tectonic activity. Mar Geol, 346: 165–182
Wang K, Bilek S L. 2014. Invited review paper: Fault creep caused by subduction of rough seafloor relief. Tectonophysics, 610: 1–24
Wang P, Shan D, Wang G, Yu F, Hou J, Zhao L, Yuan Y, Fang T, Ren Z, Wang Z. 2016. Modelling and assessment of tsunami-induced vortex flows hazards from the 2011 M_W9.0 Tohoku-oki earthquake in harbors and adjacent area (in Chinese). Chin J Geophys, 59: 4162–4177
Wang W, Wang D, Wu S, Völker D, Zeng H, Cai G, Li Q. 2018. Submarine landslides on the north continental slope of the South China Sea. J Ocean Univ China, 17: 83–100
Wang X, Power W. 2011. COMCOT : A tsunami generation, propagation and run-up model. GNS Science
Wells D L, Coppersmith K J. 1994. New empirical relationships among magnitude, rupture length, rupture width, rupture area, and surface displacement. Bull Seismol Soc Am, 84: 974–1002
Wen R, Ren Y, Li X, Pan R. 2011. Probabilistic earthquake tsunami hazard assessement approach (in Chinese). South China J Seismol, 31: 1–13
Williams R, Rowley P, Garthwaite M C. 2019. Reconstructing the Anak Krakatau flank collapse that caused the December 2018 Indonesian tsunami. Geology, 47: 973–976
Wu S G, Qin Z L, Wang D W, Peng X C, Wang Z J, Yao G S. 2011. Analysis on seismic characteristics and triggering mechanisms of mass transport deposits on the Northern slope of the South China Sea. Chin J Geophys, 54: 1056–1068
Wu S, Sun Y, Li Q, Wang J, Wang D, Sun Q, Chen C, Xie Y. 2019. Deepwaer Geohazards in the South China Sea (in Chinese). Beijing: Science Press
Wu S, Wang D, Völker D. 2018. Deep-sea geohazards in the South China Sea. J Ocean Univ China, 17: 1–7
Wu T R, Huang H C. 2009. Modeling tsunami hazards from Manila trench to Taiwan. J Asian Earth Sci, 36: 21–28
Xia S, Qiu X, Tong C H, Xu H, Zhao M. 2012. Three-dimensional to-

mographic model of the crust beneath the Hong Kong region. Geology, 40: 59–62
Xia S, Zhou P, Zhao D, Cao J. 2020. Seismogenic structure in the source zone of the 1918 *M*7.5 NanAo earthquake in the northern South China Sea. Phys Earth Planet Inter, 302: 106472
Xie X, Chen C, Li L, Wu S, Yuen D A, Wang D. 2019. Tsunami hazard assessment for atoll islands inside the South China Sea: A case study of the Xisha Archipelago. Phys Earth Planet Inter, 290: 20–35
Xie Y, Cai M. 1983. Compilation of Historical Earthquakes of China (in Chinese). Beijing: Science Press
Xiong C, Cao J, Sun J, Xia S, Wan K, Fan C, Yang B. 2018. Varition characteristics along the strike of the Littoral Fault Zone in offshore Pearl River Estuary (in Chinese). Earth Sci, 43: 352–367
Xu H, Qiu X, Zhao M, Sun J, Zhu J. 2006. The charateristics of crustal structure and seismogenic zone of the NanAo earthquake (*M*=7.5) in the northeastern South China Sea (in Chinese). Chin Sci Bull, B11: 83–91
Xu H, Ye C, Qiu X, Sun J, Xia S. 2010. Deep geophysical survery and investigation of the seismogenic structure of the Littoral Fault Zone in the nothern South China Sea (in Chinese). South China J Seismol, 30: 10–18
Xu Q. 2007. Land sinking into the sea and possible tsunami triggered by the 1605 Qiongzhou earthuake (in Chinese). Acta Oceanol Sin, 29: 146–156
Yang J, Li L, Zhao K, Wang P, Wang D, Sou I M, Yang Z, Hu J, Tang X, Mok K M, Liu P L F. 2019. A comparative study of Typhoon Hato (2017) and Typhoon Mangkhut (2018)—Their Impacts on coastal inundation in Macau. J Geophys Res-Oceans, 124: 9590–9619
Yang W, Sun L, Yang Z, Gao S, Gao Y, Shao D, Mei Y, Zang J, Wang Y, Xie Z. 2019. Nan'ao, an archaeological site of Song dynasty destroyed by tsunami (in Chinese). Chin Sci Bull, 64: 107–120
Yang W, Xiew Z, Sun L. 2021. Research progress in the reconstruction of paleotsunami in the South China Sea and the tsunami deposit characteristics (in Chinese). Earth Sci Front, 28: 246–257
Yang X, Peel F J, McNeill L C, Sanderson D J. 2020. Comparison of fold-thrust belts driven by plate convergence and gravitational failure. Earth-Sci Rev, 203: 103136
Yang X. 2003. Summarization of genesis of low-velocity layer in contiental crust (in Chinese). Geol Sci Tech Inform, 22: 35–41
Yao B. 1993. Cenozoic tectonics of the continental margins in northern South China Sea (in Chinese). GeolStudy South China Sea, 5: 1–12
Yavari-Ramshe S, Ataie-Ashtiani B. 2019. On the effects of landslide deformability and initial submergence on landslide-generated waves. Landslides, 16: 37–53
Ye L, Kanamori H, Rivera L, Lay T, Zhou Y, Sianipar D, Satake K. 2020. The 22 December 2018 tsunami from flank collapse of Anak Krakatau volcano during eruption. Sci Adv, 6: eaaz1377
Yokota Y, Ishikawa T, Watanabe S I, Tashiro T, Asada A. 2016. Seafloor geodetic constraints on interplate coupling of the Nankai Trough megathrust zone. Nature, 534: 374–377
Yu F, Dong J, Xu F. 2016. Offshore Oceanography in China: Marine Hazards (in Chinese). Beijing: China Ocean Press
Yu F, Yuan Y, Wang P, Xu Z, Zhao L, Hou J, Wang J, Li H, Fan T, Gao Y, Ren Z, Sun L, Wang Z, Shi J. 2020. Modern Technologies in Earthquake-Generated Tsunami Early Warning (in Chinese). Beijing: Science Press
Yu S B, Kuo L C, Punongbayan R S, Ramos E G. 1999. GPS observation of crustal deformation in the Taiwan-Luzon Region. Geophys Res Lett, 26: 923–926
Yuan Y, Li H, Wei Y, Shi F, Wang Z, Hou J, Wang P, Xu Z. 2021. Probabilistic tsunami hazard assessment (PTHA) for southeast coast of Chinese Mainland and Taiwan Island. J Geophys Res-Solid Earth, 126: e20344
Yue H, Zhang Y, Ge Z, Wang T, Zhao L. 2020. Resolving rupture processes of great earthquakes: Reviews and perspective from fast response to joint inversion. Sci China Earth Sci, 63: 492–511
Zengaffinen T, Løvholt F, Pedersen G K, Harbitz C B. 2020. Effects of rotational submarine slump dynamics on tsunami genesis: New insight from idealized models and the 1929 Grand Banks event. Geol Soc Lond Spec Publ, 500: 41–61
Zhang C, Kirby J T, Shi F, Ma G, Grilli S T. 2021a. A two-layer non-hydrostatic landslide model for tsunami generation on irregular bathymetry. 1. Theoretical basis. Ocean Model, 159: 101749
Zhang C, Kirby J T, Shi F, Ma G, Grilli S T. 2021b. A two-layer non-hydrostatic landslide model for tsunami generation on irregular bathymetry. 2. Numerical discretization and model validation. Ocean Model, 160: 101769
Zhao M, Qiu X, Xia K, Ye C. 2003. Research progress and future prospects of the Littoral Fault Zone in the notheastern South China Sea (in Chinese). South China J Seismol, 23: 20–27
Zhao M, Qiu X, Ye C, Xia K, Huang C, Xie J, Wang P. 2004. Analysis on deep crustal structure along the onshore-offshore seismic profile across the Binhai (Littoral) Fault Zone in northeastern South China Sea (in Chinese). Chin J Geophys, 47: 845–852
Zhong J. 1987. Investigation of the location and activiation of the Littoral Fault Zone (in Chinese). South China J Seismol, 7: 4–10
Zhou Q, Li X, Zhou H, Liu L, Xu Y, Gao S, Ma L. 2018. Characteristics and genetic analysis of submarine landslides in the northern slope of the South China Sea. Mar Geophys Res, 40: 303–314
Zhu J, Li S, Sun Z, Li X, Li J. 2017. Crustal architecture and subduction processes along the Manila Trench (in Chinese). Earth Sci Front, 24: 341–351
Zhu J, Sun Z, Kopp H, Qiu X, Xu H, Li S, Zhan W. 2013. Segmentation of the Manila subduction system from migrated multichannel seismics and wedge taper analysis. Mar Geophys Res, 34: 379–391

(Responsible editor: Ling CHEN)